Perceiving SARS-CoV2 Mpro and PLpro dual inhibitors from pool of recognized antiviral compounds of endophytic microbes: an in-silico simulation study

Jignesh Prajapati
Gujarat University
Rohit Patel
Gujarat University
Priyashi Rao
Gujarat University
Meenu Saraf
Gujarat University
Rakesh Rawal
Gujarat University
Dweipayan Goswami (dweipayan.goswami@gujaratuniversity.ac.in)
Gujarat University

Research Article

Keywords: SARS-CoV-2, Antiviral, Papain-like protease (PLpro), Main protease (Mpro), endophytes, Molecular dynamics simulation

Posted Date: August 23rd, 2021

DOI: https://doi.org/10.21203/rs.3.rs-829046/v1

Perceiving SARS-CoV2 Mpro and PLpro dual inhibitors from pool of recognized antiviral compounds of endophytic microbes: an *in-silico* simulation study

Jignesh Prajapati[1#], Rohit Patel[2#], Priyashi Rao[1], Meenu Saraf[2], Rakesh Rawal[1], Dweipayan Goswami[2*]

[1]Department of Biochemistry & Forensic Science, University School of Sciences, Gujarat University, Ahmedabad 380009, Gujarat, India.

[2]Department of Microbiology & Biotechnology, University School of Sciences, Gujarat University, Ahmedabad 380009, Gujarat, India.

Jignesh Prajapati (ORCID: 0000-0001-8700-9929)

Rohit Patel (ORCID: 0000-0002-7077-4218)

Priyashi Rao (ORCID: 0000-0002-7203-8249)

Meenu Saraf (ORCID: 0000-0003-4964-9452)

Rakesh Rawal (ORCID: 0000-0002-7985-1187)

Dweipayan Goswami (ORCID: 0000-0003-0165-0294)

[#] Jignesh Prajapati and Rohit Patel have contributed equally and are equal first authors.

***Details of correspondence**

Dr. Dweipayan Goswami

Assistant Professor,

Department of Microbiology & Biotechnology,

University School of Sciences, Gujarat University,

Ahmedabad 380009, Gujarat, India

Email: dweipayan.goswami@gujaratuniversity.ac.in

Authors Approval

All authors have seen and approved the manuscript.

Abstract

The enormous impact of SARS-CoV2 continues and scientific community is seeking to discover the tactics to impede the spread of virus. The essential result is attenuated, and genetically engineered vaccines are being driven into the market with the general effectiveness being around 80%. Therefore, vaccination is not the sole answer for combat this pandemic. The substitute methodology is adapted to target on this virus with a medication in blend with existing vaccines. Papain like protease (nsp-3; nonstructural protein) and Mpro (nsp-5; nonstructural protein) of novel corona virus are the ideal target to develop drugs as they play different roles that are essential for viral development and replication. Utilizing computational methodology, we plan to distinguish a plausible microbial metabolite as analogue of GRL0617 (the well-established inhibitor of PLpro) and X77 (the well-established inhibitor of Mpro) from the pool of known antiviral compounds of endophytic microbes to interact and inhibit PLpro and Mpro as dual inhibitors. In the wake of collecting known antiviral compounds of endophytic microbes and screened them through pharmacophore hypothesis, molecular docking, and dynamics simulation, we perceive Cytonic acid A and Cytonic acid B to be seen as the potent PLpro and Mpro dual inhibitors using rigorous computational methods.

Keywords: SARS-CoV-2; Antiviral; Papain-like protease (PLpro); Main protease (Mpro); endophytes; Molecular dynamics simulation

Introduction

Coronavirus disease 19 (COVID-19) is a new SARS-CoV2 linked disease that manifests as a range of clinical signs going from asymptomatic, minor influenza like manifestations to acute respiratory distress, pneumonia, and demise [1,2]. COVID-19 pandemic shown up over eighteen months prior and flipped around our lives. During the first wave of the infection, all affected countries endorsed various precautionary measures, including a total or partial lockdown of residents, instructed social distancing, wearing of face masks, and frequent hand sanitization. More significantly, individuals did not follow the prevention measures precisely and the number of affected individuals changed relying upon how powerful the prevention measures were; however, it never went to naught. Additionally, these recommended measures have been headed to the detriment of the economy and more crucially, these severe control measures alone are not viable enough to stop the COVID-19 pandemic. This is vividly observed in both developing and developed countries, where people were hit by a third wave of corona virus infection due to a lack of antiviral medication or vaccination, and as a result, the scientists from around the world are prompted to find effective medications and vaccines for COVID-19 treatment and prevention[1,3].

In last one year, COVID-19 vaccines are being developed using various strategies, rendered from typical inactivated and live attenuated vaccines to more innovative messenger RNA (mRNA) and DNA technologies, like viral vector and subunit vaccines[4–6]. For instance, BBV152 is a classical inactivated whole virion vaccine while, mRNA-1273 and mRNA-BNT162b2 are mRNA-based vaccines that target SARS-CoV2 spike protein[5]. Herd immunity may hypothetically be achieved because of the high incidence of protection from infection after vaccination. Besides, there are yet various vaccination related inquiries that presently unaddressed, include the length of a vaccination preventive effects and cross-protection against viral variants (Alpha, Beta, Gamma, Delta, Delta Plus, Epsilon, Eta, Theta, Iota, Kappa, and Lambda), particularly new mutations [7]. New cases of COVID-19 are dropping as vaccination rates rise, but the list of variants is probably going to grow as new mutation develops, which is the reason using vaccines to tackle the pandemic still has a long way to go [8].

Until vaccine-induced herd immunity is established, another promising strategy would be to foster new drugs that are compelling against SARS-CoV2. Virus replication necessitates a certain set of structural and non-structural proteins. Absence of these proteins can limit host-to-host transfer or replication, culminating in virus spread suppression. As a result, medicines that can regulate the accessibility of these proteins should be pursued. SARS-CoV2 has a 30-kb RNA genome that encodes two large overlapping polyprotein precursors (pp1a and

pp1ab), which are acted on by viral proteases like Main protease (Mpro) and Papain-like protease (PLpro) to generate 16 non-structural proteins (NSPs) involved in viral replication, transcription, and assembly of the virus nuclear material into the capsid protein coat (Figure 1). Consequently, inhibiting these proteases may have a considerable impact on the viral machinery and the overall rate of viral infection. Scientist around the globe have well considered these proteases (Mpro and PLpro) as important drug targets for developing medications as inhibiting these proteases directly halts the functioning and replication of SARS-CoV2, making the virus feeble.

Bioactive and natural products derived from plants, microorganisms, and animals have long been recommended to treat infectious and non-infectious disorders, and they keep on assuming a significant part for drug development in the wake of this twenty-first-century pandemic [9]. The likelihood of discovering novel medications using metagenomic databases of natural compounds has increased as computer hardware and software technologies has progressed. Several investigations have used advanced computational tools such as docking, molecular dynamics simulation, and a combination of advanced silico approaches to find natural compounds from large database that could be used as possible lead compounds [10–13]. However, this is like looking for a needle in a haystack while trying to discover the suitable molecule from a large database. The use of a specific library of small compound could aid in the exploration of the suitable molecule. Antiviral metabolites from endophytic origin are still not investigated against the SARS-CoV2 proteases (Mpro and PLpro), consequently they can be used as a source for specified small compound library.

Endophytes are microorganisms that live within plant tissues with mutualistic association for at least part of their life cycle without causing any apparent disease manifestation [14]. Research on endophytic fungi have evinced that, they are an auspicious resource of bioactive compounds and to access this valuable source, the diversity of endophytic fungi and their species richness in different parts of world has been explored. Large number of secondary metabolites, especially from fungal endophytes are extracted, isolated, and characterized, such as Emodin, ω-hydroxyemodin, (+)-Sclerotiorin, Phomopsone B and Phomopsone C, which possess viral protease inhibition activity [15–18].

In present study, we have manually curated previously recognized antiviral compounds obtained from endophytic microorganisms and prepared a library to endeavoured to virtually screen them as a dual inhibitor for Mpro and PLpro with therapeutic potential to act simultaneously on the activity of both proteases. Cytonic acid A and Cytonic acid B were selected as dual protease inhibitor after pharmacophore screening, molecular docking, ADMET (Absorption–Distribution–Metabolism–Excretion–Toxicity) profile and binding energy

calculation through MM-GBSA assay. Moreover, to analyze the nature of ligand-protein interaction, a 100ns molecular dynamic (MD) simulation was undertaken for Cytonic acid derivatives and control compounds under simulated physiological conditions. We anticipate that Cytonic acid A and Cytonic acid B as dual-target therapeutic approach for COVID-19 could be more effective and would substantially reduce the use of combinational drugs as well as the multi-drug dose load in the host system.

Materials and methods

Protein preparation

PLpro protein of SARS-CoV2 (PDB ID: 7CMD) co-crystalized form with GRL0617 and Mpro of SARS-CoV2 (PDB ID: 6W63) co-crystalized form with X77 were retrieved from protein databank (PDB) [19–21]. Here, GRL0617 and X77 are the known inhibitors for respective proteins and were used as reference. Proteins were imported to Schrödinger Maestro and were prepared in *Protein preparation wizard (PrepWizard)* of Maestro. In which, each of the protein was first pre-processed by adding hydrogens, converting selenomethionines to methionines and het states were generated Epik for pH 7.0. In the next step of protein preparation, H-bond assignment was done using PROPKA for pH 7.0 for optimizing the protein. Once the protein was optimized, the restrained minimization of protein was done using OPLS2005 (Optimized Kanhesia for Liquid Simulations) force field.

Meta data curation for Ligand Library development

Electronic databases such as PubMed, Science Direct, Scopus and Google Scholar were used for data collection of endophytic microorganisms and its bioactive metabolites. Based on experimental antiviral effects of metabolites against various viruses such as influenza, H1N1, HIV, HCV, and EV-71, the 45 antiviral compounds were retrieved from published studies. Table 1 lists the 45 compounds present in the library, along with their isolation sources and bioactivity. All the ligands were retrieved in SDF format and were imported to the Schrödinger Maestro for ligand preparation for docking. *LigPrep* wizard in Schrödinger Maestro was used to generate ionization states for each ligand structure with Epik at a physiological pH of 7.2 ± 0.2 unit. Rest other options were kept as default and the ligands were minimized under OPLS2005 force field. The output files prepared on ligand minimization was used for docking using Glide.

Generation of E-pharmacophore model

An energy-optimized pharmacophore (E-pharmacophore) hypothesis was generated separately using the crystal structure of (i) SARS-CoV-2 PLpro bound to an inhibitor GRL0617 with a resolution of 2.1 Å (PDB ID: 7CMD) and (ii) SARS-CoV-2 Mpro bound to an inhibitor

X77 with a resolution of 2.1 Å (PDB ID: 6W63). During pre-processing of the complex, water molecules within 5 Å distance of the ligand were eliminated from the structure and then minimized complex was used to develop E-pharmacophore model [34,35]. *'Develop Pharmacophore from Protein-Ligand Complex'* option in the Phase module was used to create the E-pharmacophore model. The minimized complex was then imported into the workspace, where default pharmacophore properties like hydrogen bond acceptor (A), hydrogen bond donor (D), aromatic ring (R), and hydrophobicity (H) were mapped. The functional groups in the bioactivity of the targeted enzyme (PLpro) are included in the generated pharmacophore hypothesis. On performing E-Pharmacophore, two hypotheses were generated one for each protein-ligand complex. These E-Pharmacophore hypothesis were then used for screening of ligands.

E-pharmacophore based virtual screening

A pharmacophore-based virtual screening for prepared library of 45 compounds was carried out using the Phase module of the Schrodinger suite to develop a collection of compounds with the requisite molecular characteristics for optimal binding to PLpro and Mpro, as mapped by the selected E-pharmacophore models.

Molecular Docking

The optimized and minimized proteins from the previous step were used for docking. The first step for docking is to prepare the grid at the exact same co-ordinates as that of native ligand GRL0617 in 7CMD for PLpro and X77 in 6W63 for Mpro. The grid for PLpro was developed at the co-ordinates, X -34.22, Y -11.61, Z -30.05, with the size 10 Å X 11 Å X 14 Å while for Mpro, grid was developed at the co-ordinates, X -20.58, Y 18.1, Z -26.98, with the size 12 Å X 14 Å X 15 Å, using '*Receptor grid generation'* feature of Glide module in Schrödinger Maestro. For docking, the output file of (i) receptor grid generation and (ii) minimized ligands obtained after E-pharmacophore based screening (15 for PLpro and 18 for Mpro) were imported in the 'Ligand docking' window of Glide module in Schrödinger Maestro. Moreover, native ligand GRL0617 for PLpro and X77 for Mpro were used as positive controls for docking with respective proteins, PLpro and Mpro. Under the settings, the precision of docking was set as 'Extra Precision (XP)', Ligand sampling was set as 'Flexible' and the Epik state penalties were added to docking score. After docking, single pose with minimum binding energy (kcal/mol) was selected for further studies. Selected pose for each ligand was opened in BIOVIA Discovery Studio (DS) visualizer for analysis of interactions taking place beteween ligand and amino acids of protein. Ligands capable of producing maximum interactions with target protein like GRL0617 (for PLpro) and X77 (for Mpro), were selected for MM-GBSA assessment.

MM-GBSA calculation

Molecular mechanics generalized Born surface area (MM-GBSA) calculation was used to calculate the binding free energy change [36–39]. Docked ligand-receptor complexes were minimized using local optimization feature present in Prime wizard of Maestro (Schrödinger Release 2017-4). Binding energy for each receptor-ligand complex was determined by using OPLS-2005 force field. Equation employed for free energy calculation is as follows:

$$\Delta GBind = \Delta EMM + \Delta GSolv + \Delta GSA$$

Here, ΔEMM represents the variation between the minimized energy of the receptor–ligand complexes; ΔGSolv represents the variation between the GBSA solvation energy of the receptor–ligand complexes and the sum of the solvation energies for the protein and ligand. In ΔGSA contains some of the surface area energies in the protein and ligand and the difference in the surface area energies for the complexes. The minimization of the docked complexes was done using a local optimization feature of prime.

ADMET analysis

The ADMET properties of the GRL0617, X77 (as controls) and top screened ligands (test endophytic molecules) were predicted using the pkCSM - pharmacokinetics server [40] that predicted both physiochemical and pharmacological properties. To perform this analysis SMILES (Simplified Molecule Input Line Entry Specification) of the compounds were retrieved from PubChem and uploaded to pkCSM - pharmacokinetics server. Parameters computed by server include Water solubility in buffer system (SK atomic types, mg/L), *in-vivo* CaCO2 cell permeability (Human colorectal carcinoma), Human intestinal absorption (HIA, %), *in-vivo* P-glycoprotein inhibition and *in-vivo* skin permeability (logKp, cm/hour). Metabolic parameters were determined using *in-vivo* Cytochrome P450 2C19 inhibition, *in-vivo Cytochrome* P450 2C9 inhibition, *in-vivo* Cytochrome P450 2D6 inhibition, *in-vivo* Cytochrome P450 2D6 substrate, *in-vivo* Cytochrome P450 3A4 inhibition and *in-vivo* Cytochrome P450 3A4 substrate. Distribution property included tests like, Blood-Brain Barrier (BBB) penetration, Lipinski's Rule (Rule of Five), Central Nervous System (CNS) permeability. To access the toxicity of compounds under study a range of important endpoints including, Acute algae toxicity, Ames test, two years carcinogenicity bioassay in mouse, two years carcinogenicity bioassay in rat, *in-vivo* Ames test result in TA100 strain (Metabolic activation by rat liver homogenate) were computed. Excretion again is an especially important parameter and as many drugs often withdrawn at clinical trial stages due to their poorer renal clearance. In this study we included Total Renal clearance and Renal OCT2 Substrate to identify Excretion efficacy of the proposed metabolite.

Validation Through MD Simulation

Desmond (Schrödinger Release 2018-4) by D.E. Shaw research was used to perform simulation of SARS-CoV2 PLpro Mpro in the presence of various ligands. As Cytonic acid A and Cytonic acid B were having good binding energy, proper ADMET profile and able to mimic interactions of native ligand with PLpro as well as Mpro, MD simulation was carried out for following complexes: (I) PLpro-GRL0617, (II) PLpro-Cytonic acid A, (III) PLpro-Cytonic acid B, (IV) Mpro-X77, (V) Mpro-Cytonic acid A and (VI) Mpro-Cytonic acid B. To ensure the accuracy of results of MD simulation, PLpro-GRL0617 and Mpro-X77 complexes were used as control set and results produced by Cytonic acid A and Cytonic acid B with both the proteins were compared with it. For preparation of complexes and apply pre-simulation protein relaxation, *Protein Preparation Wizard* was used. Parameters for simulation were kept as following: solvent model: TIP3P; box shape: orthorhombic; with the buffer space around the periphery of protein as 10Å. Once these parameters were defined Cl^- or Na^+ counter ions were added to perform neutralization. Steepest descent energy minimization was performed, and the simulation was proceeded for 100 ns with NPT (constant Number of particles, Pressure, and Temperature) with 300 K and 1.01 bar, constant volume, Smooth Particle Mesh Ewald (PME) method. After simulation, simulation interaction diagram wizard was used to evaluate the trajectories for root mean square deviation (RMSD), root means square fluctuation (RMSF), Ligand-protein contact profiles, and for Ligand & Protein modifications.

Results

Meta data assessment for ligand library development

The prepared library for this *in silico* analysis included a specialised library composed of 45 compounds of endophyte origin with *in vitro* anti-viral activity against various viruses such as influenza, H1N1, HIV, HCV, and EV-71. Table 1 contains the library, which includes the names of the compounds, their endophyte sources, and antiviral efficacy against particular viruses.

Structure-based pharmacophore modelling

Receptor-pharmacophore based on the 3D structure of a target protein can provide detailed and accurate information on ligand interaction attributes. H-bond donors, acceptors, positive and negative ionizable groups, lipophilic regions, and aromatic rings are the most commonly used descriptors in pharmacophore modelling. The most successful 3D structure-based e-pharmacophores were made utilizing the receptor–ligand pharmacophore generation procedure employed in PHASE, which was used to discover potentially essential amino acids implicated in ligand binding for a co-crystal GRL0617 inhibitor within the binding site of PLpro

(Figure 2a) and for a co-crystal X77 inhibitor within the binding site of Mpro (Figure 2c). H-bond acceptor, H-bond donor, and pi–pi stacking of aromatic ring was among the five key 3D attributes of the generated e-pharmacophore for the evaluated protein. Figure 2b depicts the five 3D pharmacophore characteristics for PLpro-GRL0617 complex, which include two donor hydrogen bonds, one acceptor hydrogen bond, and one aromatic ring sphere while, Figure 2d depicts the five 3D pharmacophore characteristics for Mpro-X77 complex, which include two acceptor hydrogen bond, and three aromatic ring spheres.

Pharmacophore-based virtual screening analysis

The 45 potential anti-viral compounds of endophytes origin (Table 1) were screened using the e-pharmacophore hypothesis created from the GRL0617-PLpro complex and X77-Mpro. The PHASE screen score and corresponding binding sites variables were used to filter these substances. Execution of proposed pharmacophore hypothesis, a total of 15 molecules managed to pass this filter for PLpro-GRL0167 complex (Table 2) and 18 molecules for Mpro-X77 complex (Table 3).

Molecular Docking analysis

For the first set of docking, the minimized 3D molecular structure of co-crystallized inhibitor GRL0617 was docked into the active site of viral PLpro after successive defining of the grid box utilizing Glide's Receptor Grid Generation tool in Maestro. Investigation of the co-crystallized inhibitor (GRL0617) revealed its molecular interaction with the binding site of viral protease SARS-CoV2-PLpro. Generally, the hydrophobic interactions drive the binding of GRL0617 with PLpro of SARS-CoV2 that confers inhibition of protein. The 1-naphthyl moiety of the aromatic rings frames the major contact as a pi-pi interaction with Tyr264 and Tyr268, is somewhat less presented to solvent and fits in to the cavity at the locus that oblige the leucine at the P4 position. Besides, the 1-naphthyl moiety interacts with the side chains of Pro247 and Pro248. The (R)-methyl group at GRL0167's stereocenter places itself inside the protein in the narrow area between Tyr264 and Thr301, where it fits in the limited polar space. Apart from the 1-naphthyl moiety, GRL0617 also has a single aromatic ring with – NH2 at R3 position, which is positioned at the cavity's opening. The cavity is polar owing to the presence of numerous polar groups, such as the side chain oxygens of Gln269 and the hydroxyl group of Tyr268, which essentially participate in the interaction by filling in as hydrogen bond acceptor. Total 15 microbial metabolites obtained after pharmacophore screening were considered for molecular docking investigation using Glide XP lead optimization protocol of Schrodinger suit. Four fungal metabolites of endophytic origin, Aspergilline E, Cytonic acid A, Cytonic acid B and 4-dehydroxyaltersolanol A produced significant binding energies along with multiple conserved interactions with Tyr268 of SARS-CoV2-PLpro. Each of these molecules

produced the binding energies of -7.7, -7.655, -7.292 and -6.859 kcal/mol, respectively (Table 4). The interactions between these antiviral compounds and the protein (PLpro) are depicted in Figure 3, and the structural features of GRL0617 and the top four antiviral metabolites are listed in Table 5.

Similarly, for the second set of docking, the minimized 3D molecular structure of co-crystallized inhibitor X77 was docked into the active site of viral Mpro after successive defining of the grid box utilizing Glide's Receptor Grid Generation tool in Maestro. Investigation of the co-crystallized inhibitor (X77) revealed its molecular interaction with the binding site of viral protease SARS-CoV2-Mpro. Several hydrogen bonding, pi-stacking, and hydrophobic interactions appear to be involved in the co-crystallized binding site. Non-Covalent inhibitor X77 interacts with Asn142, Gly143, Glu166 and His41 with hydrogen bond. Additionally, ligand clubbed between the benzene ring of Phe140 and the imidazole ring of His172 and forms pi-pi interaction with Cys145 and His41. Furthermore, it forms hydrophobic interaction with different amino acid present in binding site, Thr25, Leu27, Ser144, Phe140, Leu141, His172, Leu167, Tyr54, His164, Gln189, Met165 and Pro168.

The top four molecules from endophytes that showed to effectively bind with Mpro are Cytonic acid B, Cytonic acid A, Asperphenalenone D and Asperphenalenone A, respectively with the binding energy of -9.998, -9.798, -8.969 and -6.2417 (Table 4). The compound with the best docking score, Cytonic acid B makes six hydrogen bonds with the amino acids namely, Thr24, Thr26, Asn142, Glu166, Arg188 and Thr190; along with it forms pi-anion interaction with Cys145. Moreover, hydrophobic interaction in the form of alkyl/pi-alkyl interaction with His41, Met49, Met165 are being formed. Apart from these, Van der Walls interactions with this ligand is formed by 13 different amino acids as represented in the Figure 4. Cytonic acid A tends to form hydrogen bonds with Thr24, Asn142, Glu166, and Arg188, while alkyl/pi—alkyl interaction forms with Cys44, Thr26, Met49 and Met165 while forming several Van der Walls interactions with amino acids in the active site. The third best compound, based on the docking score, Asperphenalenone D makes hydrogen bonds with five amino acids, namely Thr25, Gly143, Cys145, Glu166, and Thr190. It forms hydrophobic interaction by making Alkyl/pi-alkyl interaction with His41, Met49, Met165, and Pro168 along with making Van der Walls interactions with several amino acids in the active site of Mpro. Lastly, Asperphenalenone D makes hydrogen bonds with His41, Asn119, Gly143, and Glu166; makes hydrophobic interactions in the form of alkyl/pi—alkyl interactions with Met49, Tyr118, Leu141, Cys145 and Met165. Like other ligands, this also makes Van der Walls interactions with several other amino acids in the active site of Mpro. The interactions between these antiviral compounds and the protein (Mpro) are depicted in Figure 4. Moreover, the

ligand properties of the reference inhibitors and top screened ligands of endophytic origins for both, PLpro and Mpro are represented in Table 5.

MM-GBSA analysis

Receptor-ligand interaction causes modulation of energies of both free receptor and ligand (ΔGBind) furthermore, these energies also have significant impact on stability of receptor-ligand complex. In general, negative energies represents the higher stability of any system. Various energies produced during MM-GBSA for 7CMD with native ligand GRL0617 as well as top four docking hits are presented in Table 4. Here, binding energies of GRL0617 with both 7CMD (-67.56 Kcal/mol) is in negative which suggests the higher spontaneity of interaction. Similarly, among tested compounds Cytonic acid A ranks highest in terms of stability with -58.96 Kcal/mol binding energy, whereas Cytonic acid B is the second highest ranking compound with -50.9 Kcal/mol binding energy. MM-GBSA energies of the rest of the tested compounds were also in negative but the values were relatively higher which suggest low occurrence rate for the complex. Compound Aspergilline E produced the highest docking score with SARS-CoV2-PLpro but the ΔGBind energy (-50.81 Kcal/mol) was found to be the higher than Cytonic acid derivatives.

Similarly, for Mpro, based on the ΔGBind scores of reference compound and ligands, reference ligand X77 shows the best ΔGBind score of -79.89 Kcal/mol, while of all the other test ligands of endophytic origins, Cytonic acid A has the best ΔGBind score of -75.30 Kcal/mol, followed by the Cytonic acid B, Asperphenalenone D, and Asperphenalenone A where they show the ΔGBind scores of -67.68 Kcal/mol, 65.91 Kcal/mol and 50.46 Kcal/mol respectively. Apart from ΔGBind energy, calculations for energy, Hydrogen-bonding correction, Lipophilic energy, pi-pi packing correction and Van der Waals energy is also provided in Table 6.

ADMET analysis

All the ADMET properties of the test compounds along with reference compounds GRL0617 and X77 are presented in Table 7. For any drugs to work on human body five properties play very crucial role that are absorption, distribution, metabolism, excretion, and toxicity. Property of absorption was measured using seven different models. Here, to assess the effectiveness of selected compound as oral drug CaCO2 permeability, and intestinal absorption were measured. Analysis revealed that all the compounds except Cytonic acid A and Cytonic acid B has higher values for CaCO2 permeability. However, Cytonic acid A and Cytonic acid B have 47 and 62.6 % human intestinal absorption, respectively. Moreover, assessment of skin permeability was lowest for all the tested as well as control compounds which suggest minimum absorption. To evaluate the transport of the compounds across the

membrane three tests for P-glycoprotein were performed where test compounds were tested as a substrate of the P-glycoprotein and inhibitors of the P-glycoprotein I and II. All the compounds were found to be the compatible substrates which suggests that they can pass across the membrane using ATP-binding cassette (ABC) transporter. Whereas assay as an inhibitor of P-glycoprotein I and II were found to be negative for all compounds except Aspergilline E, which highlights the inability of this compound to inhibit both these efflux pumps of foreign substances. To measure the distribution of the compounds throughout the body four assays were used namely they are volume of distribution (VDss), fraction unbound, blood brain barrier (BBB) permeability, and central nervous system (CNS) permeability. VDss assay is used to measure the total quantity of drugs needed for uniform distribution of drugs throughout the blood. Values for the assay for all the compounds were found to be lower than 0.45 log L/kg, which suggests that lower drug volume will be required. For Cytonic acid B, this value was found to be the least -1.707 log L/kg. BBB permeability of the Cytonic acid A and Cytonic acid B were found to be -1.896 and -1.782, respectively which suggests lower permeability, whereas this value for reference inhibitor GRL0617 and X77 were obtained in positive intiger values. Values for CNS permeability were also negative for all compounds under study; hence compounds are predicted to have lower permeability for CNS. Metabolism of the test drugs within body was evaluated using seven different models of cytochrome where test compounds were evaluated for their ability to act as a substrate for CYP2D6 and CYP3A4 further these compounds were assayed for the inhibition of CYP1A2, CYP2C19, CYP2C9, CYP2D6, and CYP3A4. Cytonic acid A, Cytonic acid B and all the other test compounds were found to be negative for all the seven different models of cytochrome, except for Asperphenalenone D and Asperphenalenone A predicted to interact with CYP3A4. Excretion of the compounds from the body was assessed using two models that are total clearance and renal OCT2 assay. All the test compounds and GRL0167 were found to be negative for the renal OCT2 assay hence none of them can be excreted using organic cation transporter 2 with X77 to be an only exception. Whereas total clearance assessment produces the value of 0.268 mL/min/kg for Cytonic acid A which is higher than GRL0617. Toxicity assessment was carried out with 10 different models. All the four test molecules were found to be negative for the AMES test which suggests that these compounds are not carcinogenic or mutagenic, whereas GRL0617 was reported positive for this test. For the Cytonic acid A and Cytonic acid B, maximum recommended tolerated dose values were found to be highest that is 0.44 and 0.467 log(mg/kg/day), respectively. Among the drugs hERG (human ether-a-go-go gene) I and II inhibitors are not favored as inhibition of this genes have been reported to cause QT syndrome which can lead to the fatal ventricular arrhythmia. Here, all the test compounds including control (GRL0617 and X77) were found to be negative as the inhibitor of hERG I whereas for hERG II, GRL0617 was found to be positive as an inhibitor. Oral rat acute and

chronic toxicity values for Cytonic acid A and Cytonic acid B were higher than that of GRL0617 which suggests that relatively higher doses of the compound are producing toxicity. Detailed values of the ADMET analysis are given in the Table 7.

Molecular dynamic simulations

Among the docked compounds two isomeric compounds Cytonic acid A and B, previously reported as inhibitors of human cytomegalovirus protease (hCMV), were found to be producing docking scores and MM-GBSA energies within ideal ranges for both PLpro and Mpro. Hence, both compounds were further processed using MD simulation assay to determine the protein-ligand complex stability for 100 ns. Here, along with test compound (Cytonic acid A and B), simulation of GRL0617 with SARS-CoV2-PLpro and X77 with SARS-CoV2-Mpro were also performed as a control set for respective protein.

Once MD simulation was performed, the Root Mean Square Deviation (RMSD) values for all the frames present in trajectory were calculated. In general, RMSD value of any simulation represents the modulations that take place in the state of specific atoms with reference to their initial state. Here, to generate the RMSD value docked pose of protein-ligand complex was considered as an initial state or reference pose. *Y*-axis (left) of Figure 5 and Figure 6 represents the RMSD value of protein atoms. Analysis of this plot for PLpro-GRL0617 (Figure 5) reveals that protein backbone attains the equilibration at RMSD value of 2.3 ± 0.5 Å, while Mpro-X77 (Figure 6) reveals that protein backbone attains the equilibration at RMSD value of 2.2 ± 0.6 Å. Here, the RMSD value after equilibration is not exceeding 4 Å for all the complexes under study at the peak end which is good. For the smaller and most globular proteins RMSD value is ideally supposed to be in the range of 1.0-4.0 Å. For proteins that are bigger in size this value might exceed the upper boundary limit of 4.0 Å. For the complex of PLpro-Cytonic acid A (Figure 5), RMSD value remains within the accepted limits considering the size of protein. Here, RMSD value is centered in the range of 2.0±0.5 Å and during the entire simulation RMSD value of protein remains within this range. Whereas for PLpro-Cytonic acid B, RMSD value is equilibrated at 2.3±0.5 Å. Similarly for complexes, Mpro-Cytonic acid A, and Mpro-Cytonic acid B (Figure 6) the protein backbone RMSD never exceeds 3.5 Å. In the graphs of Figure 5 right *Y*-axis represents the ligand RMSD value which provides the insight on the stability of the docked ligand pose in the binding pocket. 'Lig Fit Prot' signifies the RMSD values of ligand with reference to protein backbone. This value is ideally supposed to be in the vicinity of protein backbone RMSD value (difference of 3-4 Å) but slightly higher than that of protein RMSD value are also acceptable. Presence of significantly higher value suggests the major changes in ligand pose compared to that of docked pose. Throughout the whole simulation 'Lig Fit Prot' value of PLpro-GRL0617 (Figure 5) complex is in the range of

1.5±0.5 Å. Whereas, for the -PLpro-Cytonic acid A complex this value is found to be 5.5±1 Å although it is higher than that of protein RMSD, value is still within the acceptable range. For, PLpro-Cytonic acid B this value is 4.5±1 Å which slightly lower than that of Cytonic acid A which suggest the relatively higher stability of the complex. On the other hand, 'Lig Fit Lig' value of GRL0617 is lower than that of both Cytonic acid isomers which suggests changes in the binding pose of ligand, but the difference is not that bigger. Such results shows that GRL0617 is having relatively higher stability compared to the tested ligand in binding pocket at the given docking pose. Similarly, for Mpro-GRL0617 the 'Lig Fit Prot' values peak up to the maximum of 4.0 Å at few instances through course of simulation, while for Mpro-Cytonic acid A and Mpro-Cytonic acid B the RMSD values peaks at 6.5 Å and 7.3 Å, for Mpro-Cytonic acid A the small spike in the value from 2.5 to 6.5 Å at ~40 ns suggests the ligand reorienting and then stabilizing suggested by the RMSD value falling back to ~4.0 Å at around 55 ns (Figure 6). For all the ligands, the 'Lig Fit Prot' values attain nice plateau suggesting the interaction between protein and ligand being stable.

For the extensive study of the interactions produced during the course of simulation Figure 7 to 10 were used. Figure 7 represents the interactions made by reference ligand (GRL0617) and test compounds (Cytonic acid A and Cytonic acid B) with PLpro where the interaction types with percent interaction during 100 ns MD simulation run is represented. Similarly, for Mpro the interactions made by reference ligand (X77) and test compounds (Cytonic acid A and Cytonic acid B) is represented in Figure 8.

Figure 9 represents the interaction fraction of reference ligand (GRL0617) and test compounds (Cytonic acid A and Cytonic acid B) with PLpro while Figure 10 represents the interaction fraction of reference ligand (X77) and test compounds (Cytonic acid A and Cytonic acid B) with Mpro. Hydrogen bonds, hydrophobic interactions such as Pi cation, Pi-Pi stacking, water bridges and ionic interactions made by ligand with amino acids of proteins during 100 ns MD simulation is represented in these figures. Among these variety of interactions ionic interactions were found to be absent in both control and test ligand. For all the graphs in Figure 9 and 10, the stacked bar charts are normalized over the course of the trajectory, for example, a value of 0.7 suggests that 70% of the simulation time the specific interaction is maintained. Values over 1.0 are possible as some protein residue may make multiple contacts of same subtype with the ligand. All the bar charts in Figure 9 and 10 suggests all the ligands (reference inhibitor and test compounds) forms strong interactions with several amino acids of PLpro and Mpro respectively. At several instances the interaction fraction shoots above 0.8, which shows strong interaction of ligand with that particular amino acid.

Protein-ligand interaction timeline ligands interacting with PLpro and Mpro are represented in Figure 11 and 12 respectively. These diagrams show the instances of a ligand interacting with a particular amino acid with respect to time and with what intensity. For instance, in Figure 11, GRL0617 interacts with Pro248, Tyr264, Try268 and Gln269 strongly and evenly through the 100 ns of simulation. Similarly, Cytonic acid A and Cytonic acid B also interacts with various amino acids such as Glu161, Leu162, Asp164, Pro248, Tyr264, Tyr268, Gln269 and Tyr273 effectively. Similarly in Figure 12, X77 effectively interacts with His41, Asn142, Gly143, His163 and Glu166 of Mpro. Here like PLpro, Cytonic acid A and Cytonic acid B interacts with various amino acids of Mpro during the MD simulation. Thus, from the evidence of Docking, MM-GBSA, and MD simulations it can be deduced that Cytonic acid A and Cytonic acid B might serve as dual inhibitor of PLpro and Mpro.

Discussion

Covid consists of group of viruses known to infect humans and other animals. Biological features of this group of viruses mostly remains the same such as genomic material consists of positive strand of RNA and S-, E-, M- and N-protein are the most common protein found in all the members of the group. These viruses belong to subfamily *coronaviriae* which is further separated into four different genus that are namely, (I) Alpha Coronavirus, (ii) Beta Coronavirus, (iii) Gamma Coronavirus, (vii) Delta Coronavirus. Here, Alpha and beta coronavirus are frequently observed in humans and animals whereas gamma and delta primarily target the birds. For instance, MERS-CoV and SARS-CoV both are the Beta Coronavirus that respectively causes Middle East Respiratory Syndrome, or MERS and Serious Intense Respiratory Disorder, or SARS. Our most recent opponent SARS-CoV-2, causative agent of COVID-19, is also the member of beta coronaviruses. Apart from these viruses, Porcine Transmissible Gastroenteritis Virus (TGEV), Bovine Coronavirus (BCV), Avian Infectious Bronchitis Virus (IBV), Feline Infectious Peritonitis Virus (FIPV), Canine Coronavirus (CCoV), Porcine Hemagglutinating Encephalomyelitis Virus (HEV), and Turkey Coronavirus are also members of *coronavirinae* subfamily [1], but they are unable to infect humans as they lack the necessary S-proteins for cellular entry. MERS, and SARS- CoV have S-protein that can interact with ACE2 receptor and facilitate the viral entry in human cells [41–43]. S-proteins are specific for hosts hence cross infection is uncommon but on occasions it has been noted for instance SARS-CoV (2003) was transferred to humans from bats. Similarly, MERS-CoV (2005) was primarily infecting camels but cross infections in humans were also noted. Recently, member of Covid group, SARS-CoV2, is noted as infectious agents in humans due to cross infectivity. Moreover, such instances are more frequently occurring hence it is not farfetched to assume that it will not be the last instance of such nature [44,45].

Apart from vaccine development, scientific communities have also devoted their energies and resources to identify compounds that can counter the SARS-CoV2 virus [10,46,47]. For identification of such compounds, docking and MD simulations have been frequently utilized [2,48–50]. Variety of natural products from bacteria, fungi, and plants have been explored to inhibit the crucial viral proteins as their natural origin makes them vastly available. For instance, Pyranonigrin A, Flaviolin and Sterenin M are fungal metabolites and their docking and simulation studies with Mpro suggests that they can inhibit the viral replication via interacting with this protein [11,13,51]. Flavonoids, Dorsilurin E and Euchrenone a11 were proposed as allosteric inhibitors of Mpro[52]. Furthermore, many other studies were carried out *in silico* using molecular dynamic simulation and docking studies[53–55]. In addition, these approaches have also been utilized for potency assessment of hydroxychloroquine against various potential targets of SARS-CoV2 [56]. In all of these studies the rationale is very basic that if any of these molecule can meddle with the viral proteins then they can hinder the normal life cycle of the virus [57,58].

Endophytic microbes are symbiotically associated with plants and have been proven to produce novel or analogues of host bioactive metabolites exhibiting a variety of biological activities including antiviral activity [59]. However, compounds of specifically endophytic origin are not explored against SARS-CoV2. In the current study 45 compounds that have been reported active against viruses such as influenza, H1N1, HIV, HCV, hCMV, and EV-71 were retrieved through literature and screen them through rigorous computation workflow. Top compounds obtained after docking and MM-GBSA analysis for each protease (PLpro and Mpro) are known to have antiviral activity against different virus. Top ligands for both the proteins in present study, Cytonic acids A and B are known to possess *in vitro* inhibitory activities towards hCMV protease with the IC_{50} values of 43 µmol and 11 µmol, respectively. Both the Cytonic acids were extracted from the fermented culture of endophytic fungus *Cytonaema* sp., which was isolated from the plant *Quercus* sp. (European oak) [60]. Other compounds interacting with Mpro are Asperphenalenone A and Asperphenalenone D, which were obtained from the ethyl acetate fraction of fermented culture of *Aspergillus* sp., an endophytic fungus isolated from plant *Kadsura longipedunculata*. Asperphenalenone A and D were displayed anti-HIV activity with IC_{50}s of 4.5 and 2.4 µM, respectively [32]. Aspergilline E was extracted along with Aspergillines A-D from *Aspergillus versicolor*, an endophyte isolated from plant *Paris polyphylla* var. *yunnanensis*, collected from China. Aspergilline E showed weak antiviral activity towards Tobacco mosaic virus with IC_{50} of 33.6 ± 3.0 µM [27]. In present study it interacts with the PLpro with multiple interaction types. Another compound having strong interaction with PLpro is 4-dehydroxyaltersolanol A, which was obtained from endophytic fungus *Nigrospora* sp. YE3033, harboured in *Aconitum carmichaeli*. 4-

541 dehydroxyaltersolanol A displayed *in vitro* antiviral activity towards H1N1 influenza A with IC_{50}
542 of 8.35±1.41 µg/mL [22].

543 Cytonic acid A and Cytonic acid B are two best docked compound and their strong
544 interactions with both the proteases, PLpro and Mpro, are also shown through MD simulation
545 study. In view of unavailability of medication for corona virus infection, present study proposes
546 Cytonic acids A and B as the dual inhibitor that interact with crucial amino acids of binding site
547 of PLpro and Mpro to inhibit their function and can be beneficial in forthcoming *in vitro* and *in*
548 *vivo* studies for COVID-19 therapeutics. *In vitro* validation of the proposed compounds
549 necessitates the utilization of Biosafety Level 4 (BSL4) as we are dealing with infecting agents,
550 only *in silico* study has been carried out. Data represented in this study, will be helpful to the
551 people with such facility to validated in silico finding.

552 **References**

553 1. Shukla, A. *et al.* Curse of La Corona: unravelling the scientific and psychological
554 conundrums of the 21st century pandemic. *Mol. Divers.* (2021) doi:10.1007/s11030-
555 020-10167-2.

556 2. Fakhar, Z., Khan, S., AlOmar, S. Y., Alkhuriji, A. & Ahmad, A. ABBV-744 as a
557 potential inhibitor of SARS-CoV-2 main protease enzyme against COVID-19. *Sci.*
558 *Rep.* **11**, 1–15 (2021).

559 3. Filsinger, M., Freitag, M., Erhardt, J. & Wamsler, S. Rally around your fellows:
560 Information and social trust in a real-world experiment during the corona crisis.
561 *https://doi.org/10.1080/03623319.2021.1954463* 1–15 (2021)
562 doi:10.1080/03623319.2021.1954463.

563 4. Forni, G. *et al.* COVID-19 vaccines: where we stand and challenges ahead. *Cell*
564 *Death Differ.* **28**, 626–639 (2021).

565 5. Kyriakidis, N. C., López-Cortés, A., González, E. V., Grimaldos, A. B. & Prado, E. O.
566 SARS-CoV-2 vaccines strategies: a comprehensive review of phase 3 candidates. *npj*
567 *Vaccines* **6**, (2021).

568 6. Zahid, M. N., Moosa, M. S., Perna, S. & Buti, E. Bin. A review on COVID-19 vaccines:
569 stages of clinical trials, mode of actions and efficacy. *Arab J. Basic Appl. Sci.* **28**, 225–
570 233 (2021).

571 7. Kannan, S. R. *et al.* Evolutionary analysis of the delta and Delta Plus variants of the
572 SARS-CoV-2 viruses. *J. Autoimmun.* **124**, 102715 (2021).

573 8. Wang, P. *et al.* Antibody resistance of SARS-CoV-2 variants B.1.351 and B.1.1.7.
574 *Nature* **593**, 130–135 (2021).

575 9. Thomford, N. E. *et al.* Natural products for drug discovery in the 21st century:
576 Innovations for novel drug discovery. *Int. J. Mol. Sci.* **19**, (2018).

577 10. Messaoudi, O. *et al.* Berries anthocyanins as potential SARS-CoV–2 inhibitors
578 targeting the viral attachment and replication; molecular docking simulation. *Egypt. J.*
579 *Pet.* **30**, 33–43 (2021).

580 11. Rao, P. *et al.* Proposing a fungal metabolite-flaviolin as a potential inhibitor of 3CLpro
581 of novel coronavirus SARS-CoV-2 identified using docking and molecular dynamics.
582 *J. Biomol. Struct. Dyn.* (2020) doi:10.1080/07391102.2020.1813202.

583 12. Rao, P. *et al.* Identifying structural – functional analogue of GRL0617 , the only well -

established inhibitor for papain - like protease (PLpro) of SARS - CoV2 from the pool of fungal metabolites using docking and molecular dynamics simulation. *Mol. Divers.* (2021) doi:10.1007/s11030-021-10220-8.

13. Prajapati, J., Patel, R., Goswami, D., Saraf, M. & Rawal, R. M. Sterenin M as a potential inhibitor of SARS-CoV-2 main protease identified from MeFSAT database using molecular docking, molecular dynamics simulation and binding free energy calculation. *Comput. Biol. Med.* 104568 (2021) doi:10.1016/j.compbiomed.2021.104568.

14. Arora, D. *et al.* Isolation and characterization of bioactive metabolites from Xylaria psidii, an endophytic fungus of the medicinal plant Aegle marmelos and their role in mitochondrial dependent apoptosis against pancreatic cancer cells. *Phytomedicine* **23**, 1312–1320 (2016).

15. Hawas, U. W., El-Beih, A. A. & El-Halawany, A. M. Bioactive anthraquinones from endophytic fungus aspergillus versicolor isolated from red sea algae. *Arch. Pharm. Res.* **35**, 1749–1756 (2012).

16. Yang, Z. J. *et al.* New azaphilones, phomopsones A-C with biological activities from an endophytic fungus Phomopsis sp. CGMCC No.5416. *Fitoterapia* **145**, 104573 (2020).

17. Hawas, U. W., Al-Farawati, R., El-Kassem, L. T. A. & Turki, A. J. Different culture metabolites of the Red Sea fungus Fusarium equiseti optimize the inhibition of hepatitis C virus NS3/4A protease (HCV PR). *Mar. Drugs* **14**, (2016).

18. Arunpanichlert, J. *et al.* Azaphilone and Isocoumarin Derivatives from the Endophytic Fungus Penicillium sclerotiorum PSU-A13. *Chem. Pharm. Bull* **58**, 1033–1036 (2010).

19. Kumar, B. K. *et al.* Pharmacophore based virtual screening, molecular docking, molecular dynamics and MM-GBSA approach for identification of prospective SARS-CoV-2 inhibitor from natural product databases. *J. Biomol. Struct. Dyn.* **0**, 1–24 (2020).

20. Rao, P. *et al.* Identifying structural-functional analogue of GRL0617, the only well-established inhibitor for papain-like protease (PLpro) of SARS-CoV2 from the pool of fungal metabolites using docking and molecular dynamics simulation. *Mol. Divers.* (2021) doi:10.1007/s11030-021-10220-8.

21. Fu, Z. *et al.* The complex structure of GRL0617 and SARS-CoV-2 PLpro reveals a hot spot for antiviral drug discovery. *Nat. Commun. 2021 121* **12**, 1–12 (2021).

22. Zhang, S. P. *et al.* Antiviral anthraquinones and azaphilones produced by an endophytic fungus Nigrospora sp. from Aconitum carmichaeli. *Fitoterapia* **112**, 85–89 (2016).

23. Qin, C. *et al.* Sesquiterpenoids and xanthones derivatives produced by sponge-derived fungus Stachybotry sp. HH1 ZSDS1F1-2. *J. Antibiot. Adv. online Publ.* (2014) doi:10.1038/ja.2014.97.

24. Zhang, G. *et al.* Antiviral isoindolone derivatives from an endophytic fungus Emericella sp. associated with Aegiceras corniculatum. *Phytochemistry* **72**, 1436–1442 (2011).

25. Liu, L. *et al.* Chloropupukeananin, the first chlorinated pupukeanane derivative, and its precursors from Pestalotiopsis fici. *Org. Lett.* **10**, 1397–1400 (2008).

26. Zhang, D. *et al.* Periconiasin G, a new cytochalasan with unprecedented 7/6/5 tricyclic ring system from the endophytic fungus Periconia sp. (2016) doi:10.1016/j.tetlet.2016.01.030.

27. Zhou, M. *et al.* Aspergillines A−E, Highly Oxygenated Hexacyclic Indole−Tetrahydrofuran−Tetramic Acid Derivatives from Aspergillus versicolor. (2014) doi:10.1021/ol502307u.

28. Guo, B. *et al.* Cytonic acids A and B: Novel tridepside inhibitors of hCMV protease from the endophytic fungus Cytonaema species. *J. Nat. Prod.* **63**, 602–604 (2000).

29. Bashyal, B. P. *et al.* Altertoxins with potent anti-HIV activity from Alternaria tenuissima QUE1Se, a fungal endophyte of Quercus emoryi. *Bioorganic Med. Chem.* **22**, 6112–6116 (2014).

30. Ding, L. *et al.* Xiamycin, a pentacyclic indolosesquiterpene with selective anti-HIV activity from a bacterial mangrove endophyte. *Bioorganic Med. Chem. Lett.* **20**, 6685–6687 (2010).

31. Yu, G. *et al.* Neosartoryadins A and B, Fumiquinazoline Alkaloids from a Mangrove-Derived Fungus Neosartorya udagawae HDN13-313. *Org. Lett.* **18**, 244–247 (2016).

32. Pang, X. *et al.* Metabolites from the Plant Endophytic Fungus Aspergillus sp. CPCC 400735 and Their Anti-HIV Activities. *J. Nat. Prod.* **80**, 2595–2601 (2017).

33. Ding, J. *et al.* Microbial natural product alternariol 5-O-Methyl ether inhibits HIV-1 integration by blocking nuclear import of the pre-integration complex. *Viruses* **9**, 1–14 (2017).

649 34. Leach, A. R., Gillet, V. J., Lewis, R. A. & Taylor, R. Three-dimensional
650 pharmacophore methods in drug discovery. *J. Med. Chem.* **53**, 539–558 (2010).

651 35. Sastry, G. M., Adzhigirey, M. & Sherman, W. Protein and ligand preparation :
652 parameters , protocols , and influence on virtual screening enrichments. *J Comput*
653 *Aided Mol Des* **27**, 221–234 (2013).

654 36. Wang, W., Donini, O., Reyes, C. M. & Kollman, P. A. Biomolecular simulations:
655 Recent developments in force fields, simulations of enzyme catalysis, protein-ligand,
656 protein-protein, and protein-nucleic acid noncovalent interactions. *Annual Review of*
657 *Biophysics and Biomolecular Structure* vol. 30 211–243 (2001).

658 37. Wang, J., Hou, T. & Xu, X. Recent Advances in Free Energy Calculations with a
659 Combination of Molecular Mechanics and Continuum Models. *Curr. Comput. Aided-*
660 *Drug Des.* **2**, 287–306 (2006).

661 38. Kollman, P. A. *et al.* Calculating structures and free energies of complex molecules:
662 Combining molecular mechanics and continuum models. *Acc. Chem. Res.* **33**, 889–
663 897 (2000).

664 39. Massova, I. & Kollman, P. A. Combined molecular mechanical and continuum solvent
665 approach (MM- PBSA/GBSA) to predict ligand binding. *Perspectives in Drug*
666 *Discovery and Design* vol. 18 113–135 (2000).

667 40. Pires, D. E. V., Blundell, T. L. & Ascher, D. B. pkCSM: Predicting small-molecule
668 pharmacokinetic and toxicity properties using graph-based signatures. *J. Med. Chem.*
669 **58**, 4066–4072 (2015).

670 41. Ren, Z. *et al.* The newly emerged SARS-Like coronavirus HCoV-EMC also has an
671 'Achilles'' heel": Current effective inhibitor targeting a 3C-like protease'. *Protein Cell* **4**,
672 248–250 (2013).

673 42. Kumar, A. *et al.* Computational and In-Vitro Validation of Natural Molecules as
674 Potential Acetylcholinesterase Inhibitors and Neuroprotective Agents. *Curr. Alzheimer*
675 *Res.* **16**, 116–127 (2018).

676 43. Yang, H., Bartlam, M. & Rao, Z. Drug Design Targeting the Main Protease, the
677 Achilles Heel of Coronaviruses. *Curr. Pharm. Des.* **12**, 4573–4590 (2006).

678 44. Zhou, P. *et al.* A pneumonia outbreak associated with a new coronavirus of probable
679 bat origin. *Nature* **579**, 270–273 (2020).

680 45. Huang, C. *et al.* Clinical features of patients infected with 2019 novel coronavirus in

Wuhan, China. *Lancet* **395**, 497–506 (2020).

46. Poustforoosh, A. *et al.* Evaluation of potential anti-RNA-dependent RNA polymerase (RdRP) drugs against the newly emerged model of COVID-19 RdRP using computational methods. *Biophys. Chem.* **272**, 106564 (2021).

47. Patel, C. N., Kumar, S. P., Pandya, H. A. & Rawal, R. M. Identification of potential inhibitors of coronavirus hemagglutinin-esterase using molecular docking, molecular dynamics simulation and binding free energy calculation. *Mol. Divers.* **25**, 421–433 (2021).

48. Guedes, I. A. *et al.* Drug design and repurposing with DockThor-VS web server focusing on SARS-CoV-2 therapeutic targets and their non-synonym variants. *Sci. Rep.* **11**, 1–20 (2021).

49. Basu, A., Sarkar, A. & Maulik, U. Molecular docking study of potential phytochemicals and their effects on the complex of SARS-CoV2 spike protein and human ACE2. *Sci. Rep.* **10**, 1–15 (2020).

50. Murugan, N. A., Kumar, S., Jeyakanthan, J. & Srivastava, V. Searching for target-specific and multi-targeting organics for Covid-19 in the Drugbank database with a double scoring approach. *Sci. Rep.* **10**, 1–16 (2020).

51. Rao, P. *et al.* Reckoning a fungal metabolite, Pyranonigrin A as a potential Main protease (Mpro) inhibitor of novel SARS-CoV-2 virus identified using docking and molecular dynamics simulation. *Biophys. Chem.* **264**, 106425 (2020).

52. Jiménez-Avalos, G. *et al.* Comprehensive virtual screening of 4.8 k flavonoids reveals novel insights into allosteric inhibition of SARS-CoV-2 MPRO. *Sci. Reports 2021 111* **11**, 1–19 (2021).

53. Yoshino, R., Yasuo, N. & Sekijima, M. Identification of key interactions between SARS-CoV-2 main protease and inhibitor drug candidates. *Sci. Reports 2020 101* **10**, 1–8 (2020).

54. Keretsu, S., Bhujbal, S. P. & Cho, S. J. Rational approach toward COVID-19 main protease inhibitors via molecular docking, molecular dynamics simulation and free energy calculation. *Sci. Reports 2020 101* **10**, 1–14 (2020).

55. Komatsu, T. S. *et al.* Drug binding dynamics of the dimeric SARS-CoV-2 main protease, determined by molecular dynamics simulation. *Sci. Reports 2020 101* **10**, 1–11 (2020).

56. Mukherjee, S., Dasgupta, S., Adhikary, T., Adhikari, U. & Panja, S. S. Structural insight to hydroxychloroquine-3C-like proteinase complexation from SARS-CoV-2: inhibitor modelling study through molecular docking and MD-simulation study. *J. Biomol. Struct. Dyn.* 1–13 (2020) doi:10.1080/07391102.2020.1804458.

57. Parmar, P. *et al.* The rise of gingerol as anti-QS molecule: Darkest episode in the LuxR-mediated bioluminescence saga. *Bioorg. Chem.* **99**, 103823 (2020).

58. Pandya, P. N. *et al.* Identification of promising compounds from curry tree with cyclooxygenase inhibitory potential using a combination of machine learning, molecular docking, dynamics simulations and binding free energy calculations. *Mol. Simul.* **46**, 812–822 (2020).

59. Manganyi, M. C. & Ateba, C. N. Untapped potentials of endophytic fungi: A review of novel bioactive compounds with biological applications. *Microorganisms* **8**, 1–25 (2020).

60. Guo, B. *et al.* Cytonic acids A and B: Novel tridepside inhibitors of hCMV protease from the endophytic fungus Cytonaema species. *J. Nat. Prod.* **63**, 602–604 (2000).

Acknowledgements

We acknowledge Education Department, Government of Gujarat, India for the providing research fellowship to Rohit Patel and Priyashi Rao under the ScHeme Of Developing High quality research (SHODH), and University Grants Commission (UGC), New Delhi, India for providing the fellowship for the award of 'CSIR-NET Junior Research Fellowship (JRF)' to Jignesh Prajapati. Authors are thankful to Department of Microbiology and Biotechnology, School of Sciences, Gujarat University, DST-FIST Sponsored Department, for providing necessary facilities to perform experiments. We acknowledge GSBTM, DST, Government of Gujarat for providing Bioinformatics Node facility and Finishing School support. We acknowledge GUJCOST, DST, Government of Gujarat for Super-computing facility provision.

Author contributions

J.P. and D.G. conceived designed the experiments; J.P., R.P, and P.R. performed the experiments; J.P., R.P, and D.G. analyzed the data and wrote the manuscript; R.R, and M.S. supervised the research and revised the manuscript.

Conflicts of interest

It is declared that the authors have no conflict of interest in the publication of this article.

Funding sources

This research did not receive any specific grant from funding agencies in the public, commercial, or not-for-profit sectors.

Figures

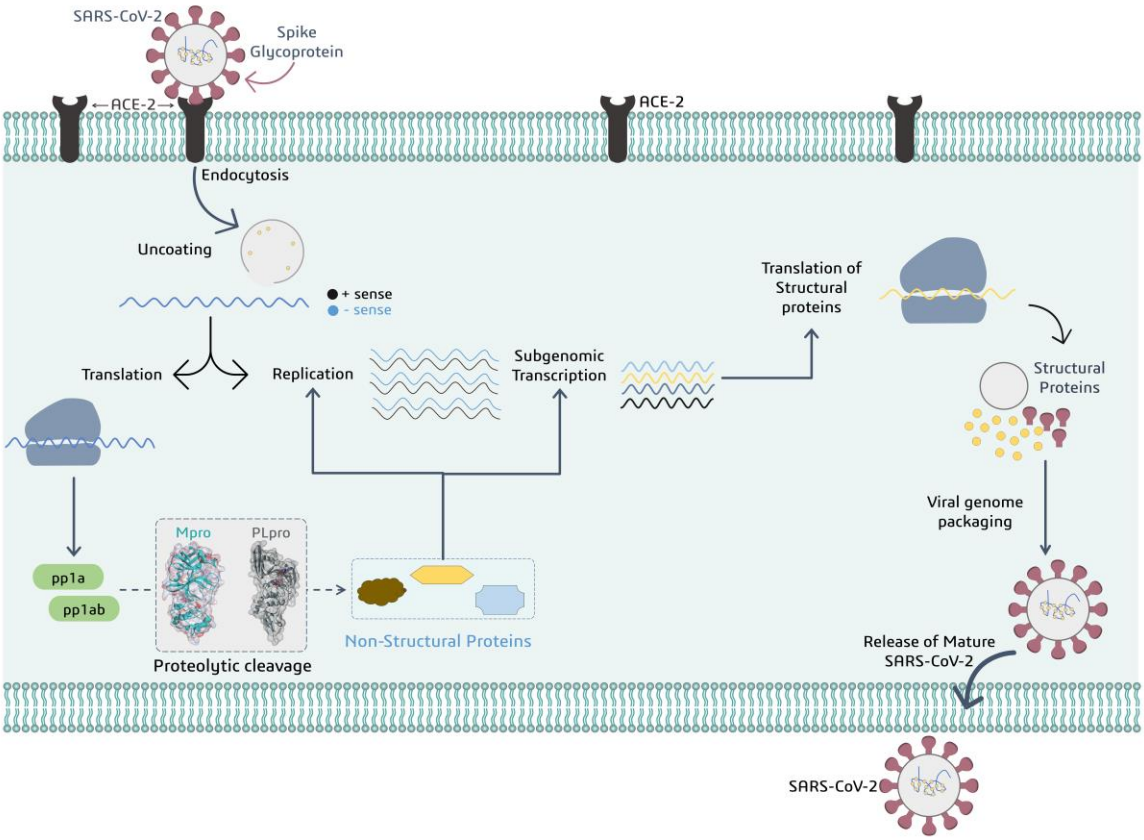

Figure 1 Representation for addressing role of viral proteases PLpro and Mpro to produce non-structural proteins participating in viral replication and transcription.

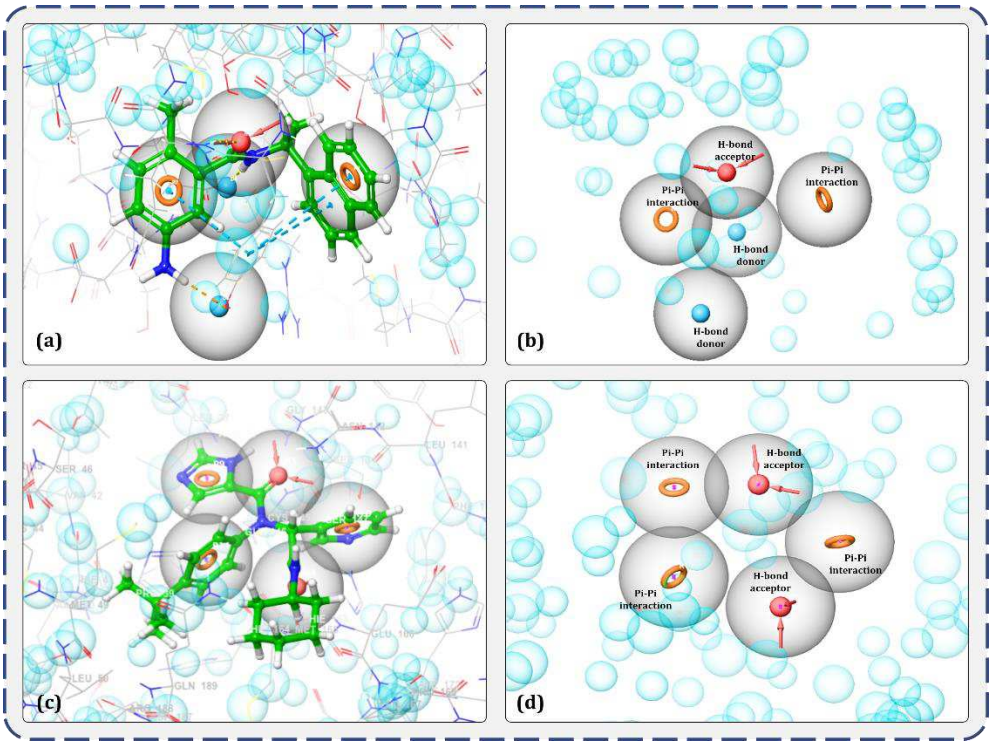

Figure 2 Illustration of E-pharmacophore features of receptor-ligand complex; (a) representative features important in binding of GRL0617 ligand with receptor PLpro and, (b) type of pharmacophore features significant for interaction with PLpro, (c) representative features important in binding of X77 ligand with receptor Mpro and, (b) type of pharmacophore features significant for interaction with Mpro.

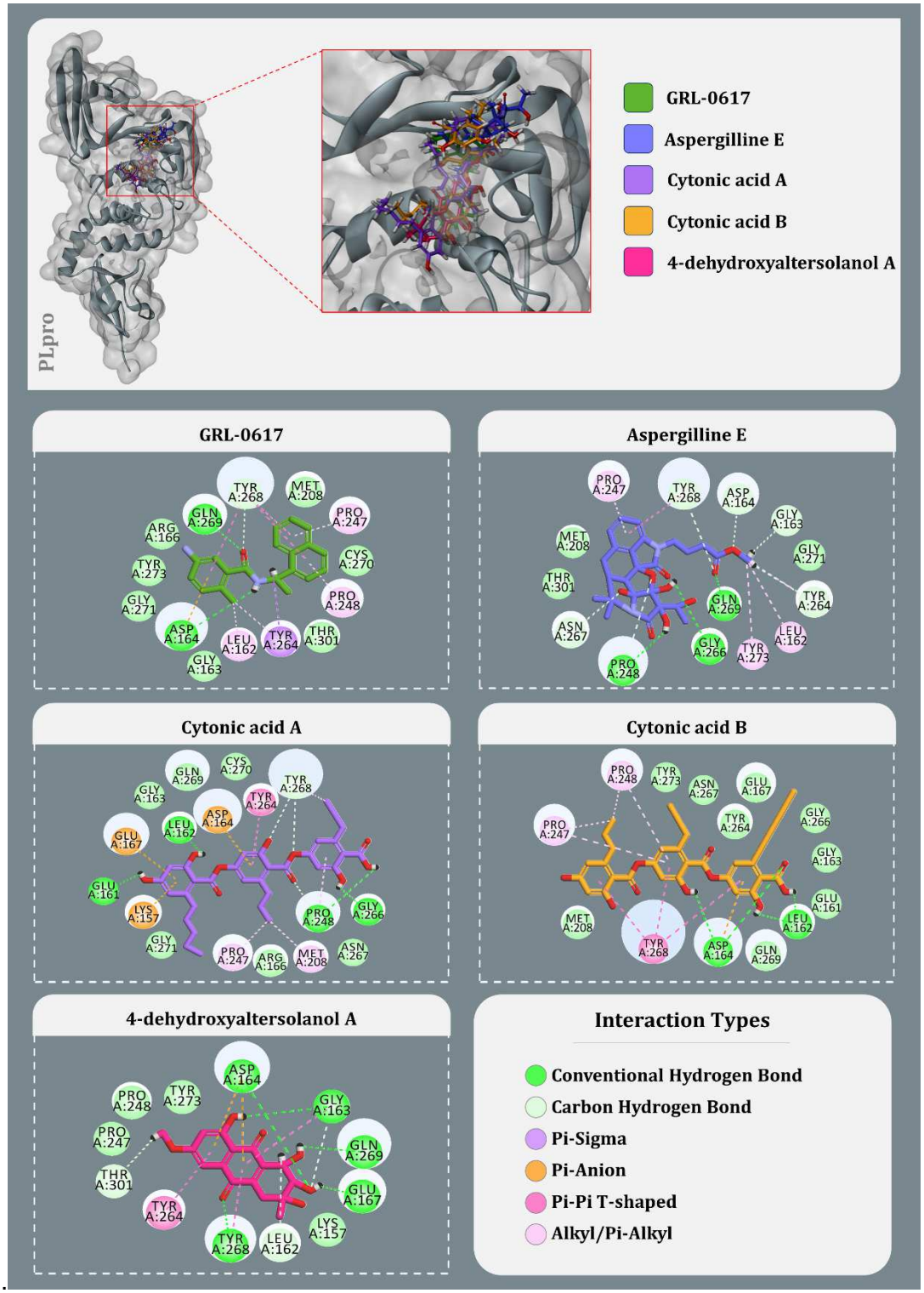

767 .

768 **Figure 3** Interaction profile of GRL0617 and best docked four antiviral compounds with SARS-
769 CoV2-PLpro (Amino acids without any bond interactions are interacting with Van der Waals
770 forces).

771

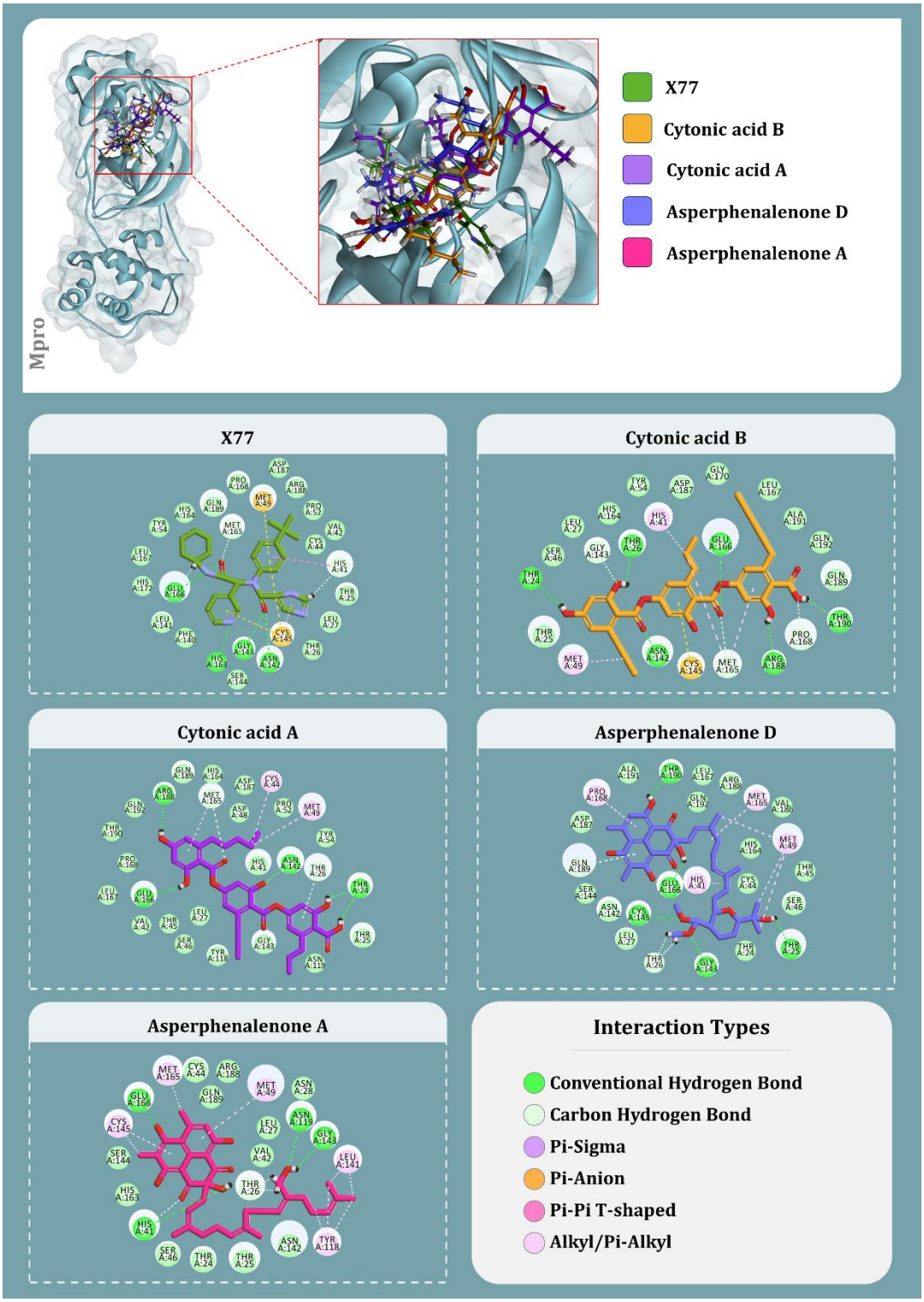

Figure 4 Interaction profile of X77 and best docked four antiviral compounds with SARS-CoV2-Mpro (Amino acids without any bond interactions are interacting with Van der Waals forces).

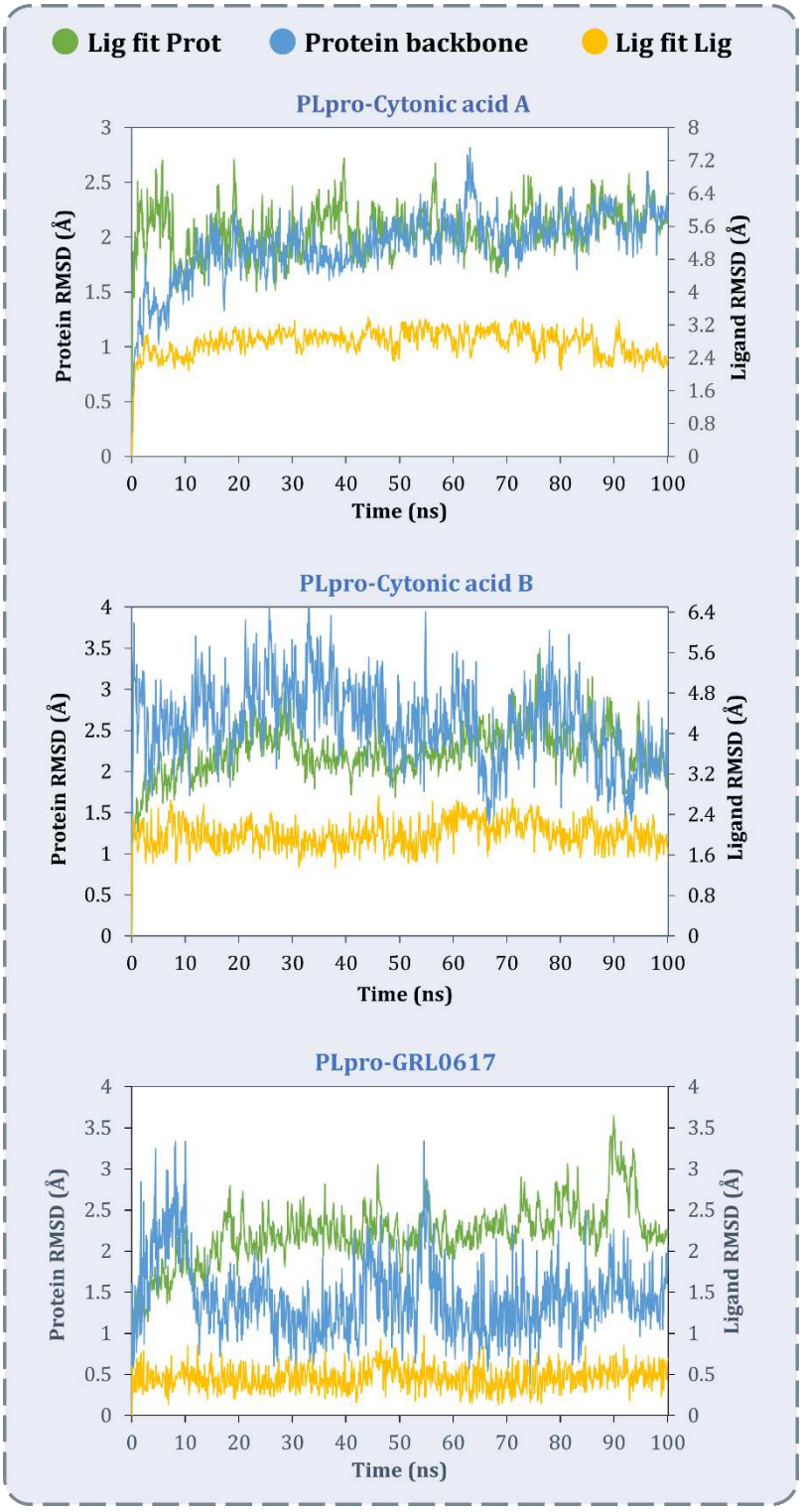

777

778

779 **Figure 5** MD simulation Protein-ligand interaction root-mean-square deviation (RMSD) profile
780 of SARS-CoV2-PLpro-Cytonic acid A, SARS-CoV2-PLpro- Cytonic acid B and SARS-CoV2-
781 PLpro-GRL0617.

782

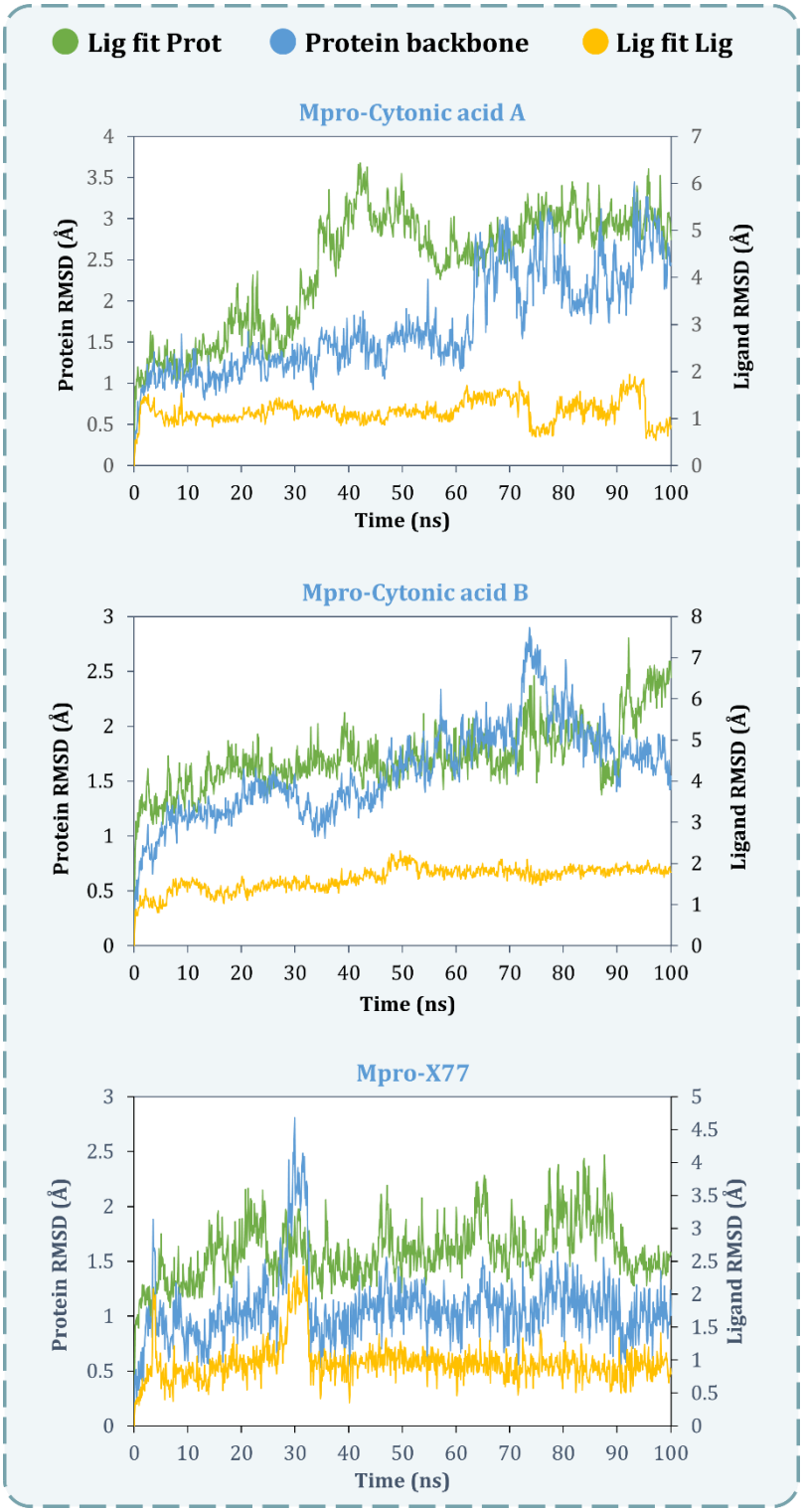

783

784 **Figure 6** MD simulation Protein-ligand interaction root-mean-square deviation (RMSD) profile
785 of SARS-CoV2-Mpro-Cytonic acid A, SARS-CoV2-Mpro- Cytonic acid B and SARS-CoV2-
786 Mpro-X77.

787

788

789

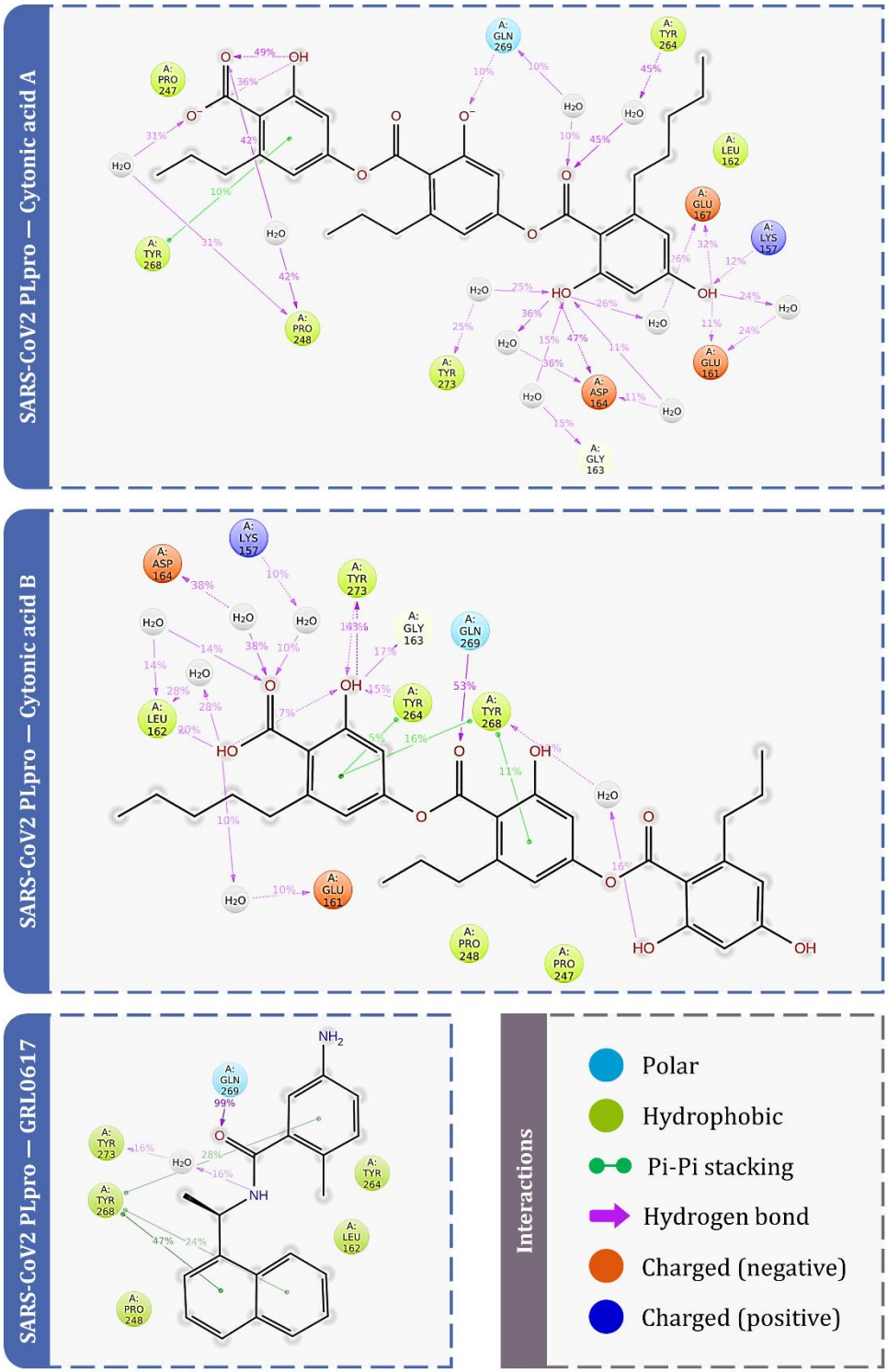

790

791 **Figure 7** Protein-Ligand interaction diagram for PLpro showing percent of total time involved
792 for particular interaction during molecular dynamics.

793

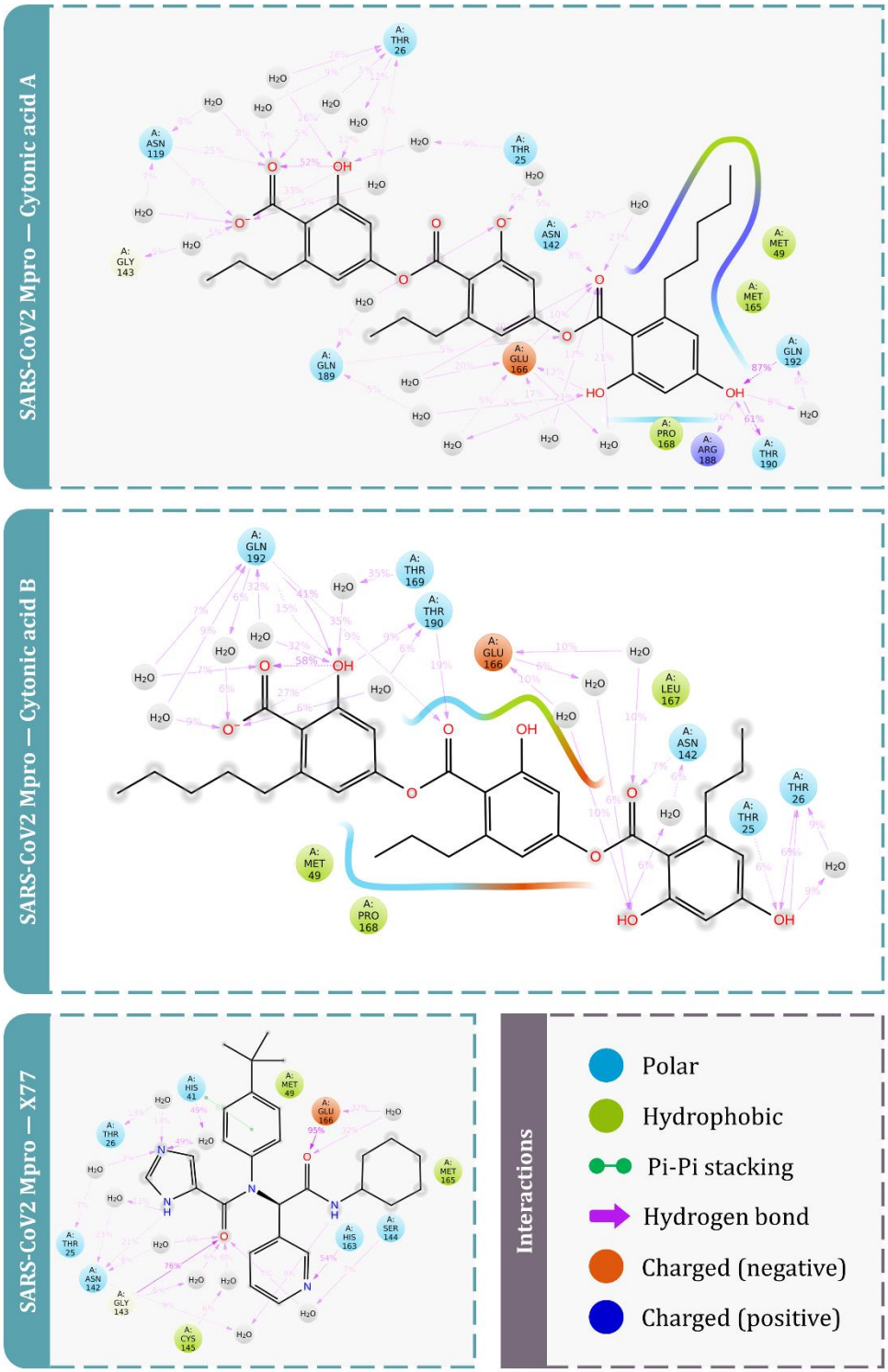

794

795 **Figure 8** Protein-Ligand interaction diagram for Mpro showing percent of total time involved
796 for particular interaction during molecular dynamics.

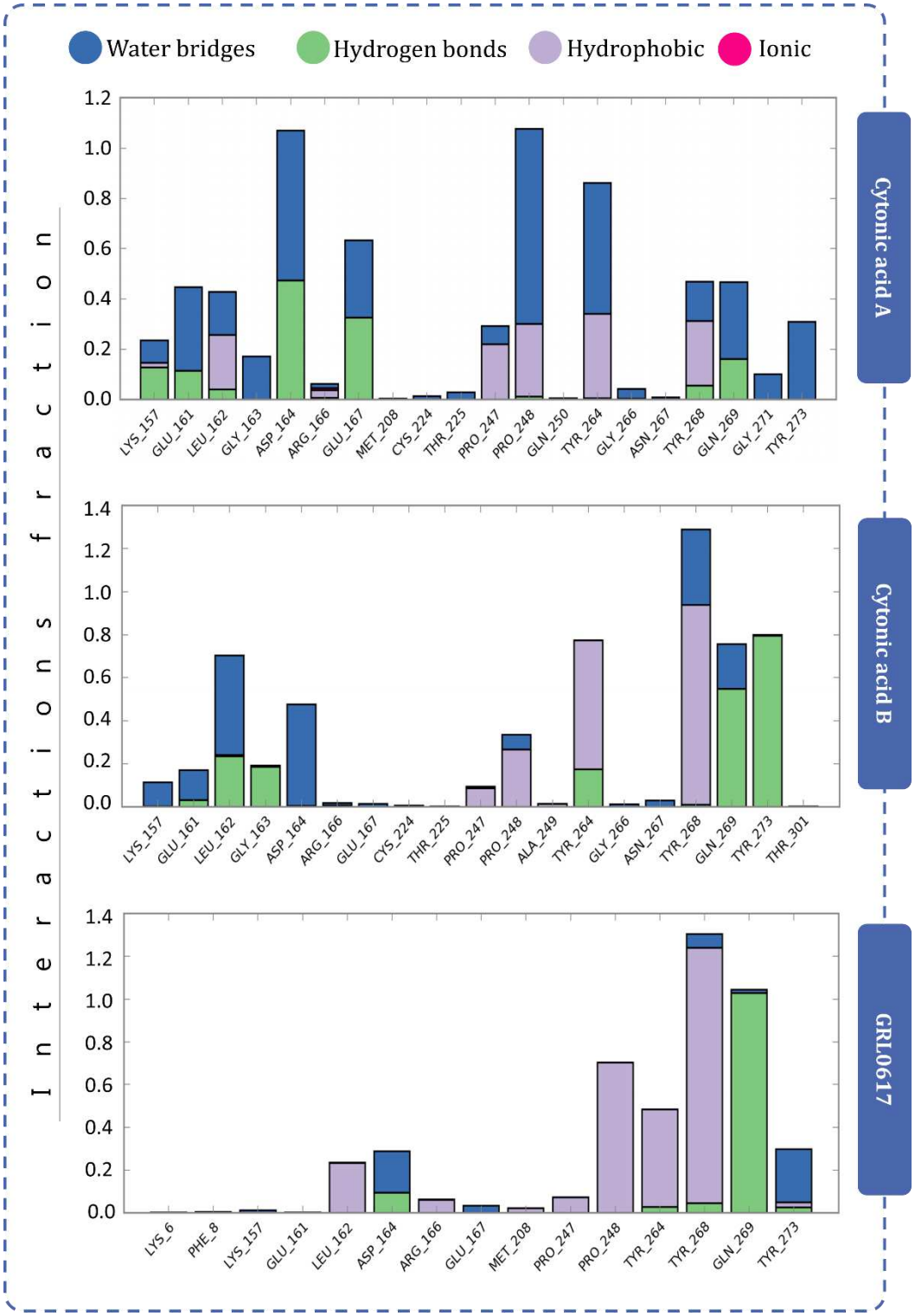

797

798 **Figure 9** Protein-Ligand interaction diagram showing interaction fraction of crucial interacting
799 amino acids of PLpro.

800

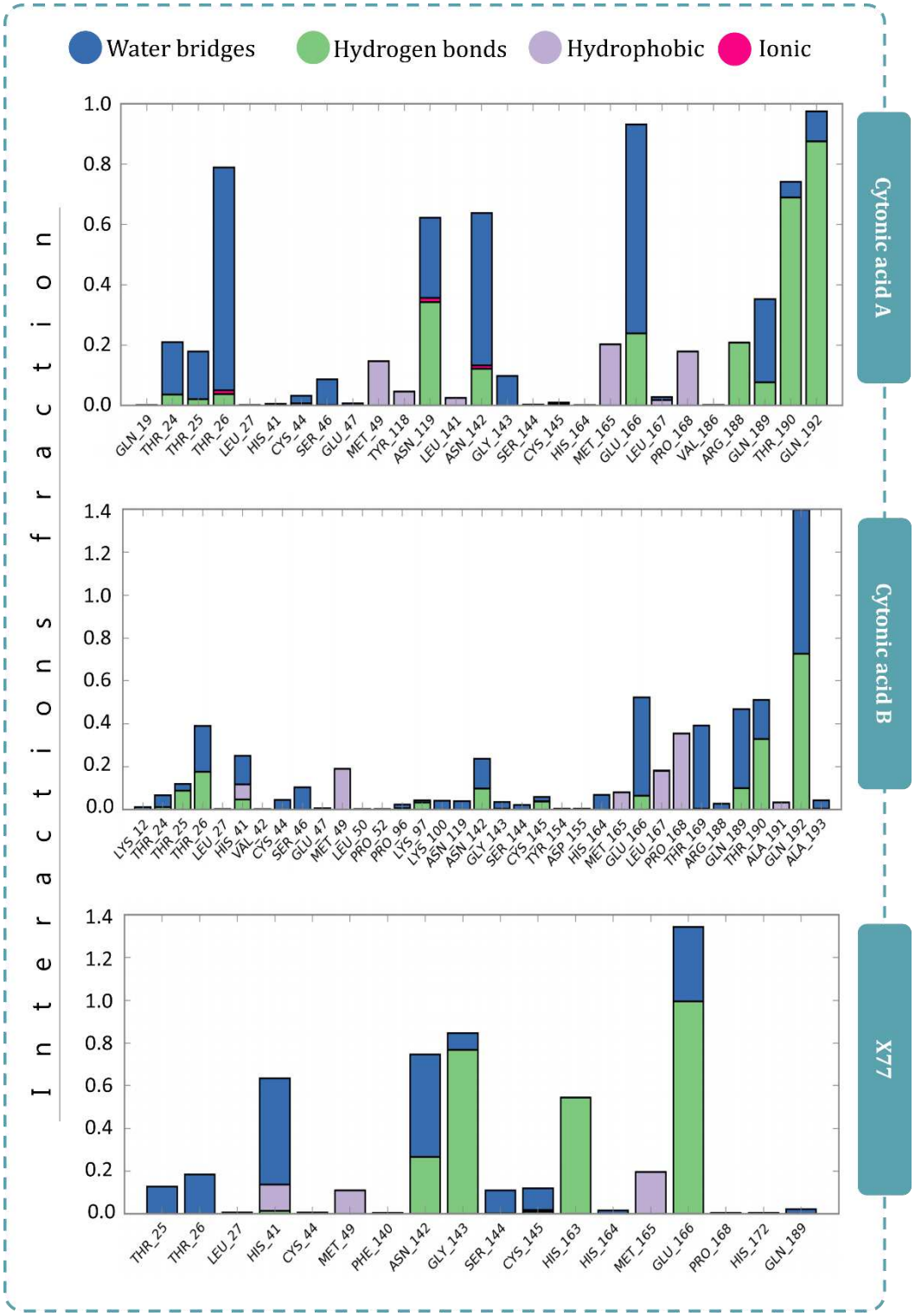

801

802 **Figure 10** Protein-Ligand interaction diagram showing interaction fraction of crucial interacting
803 amino acids of Mpro.

804

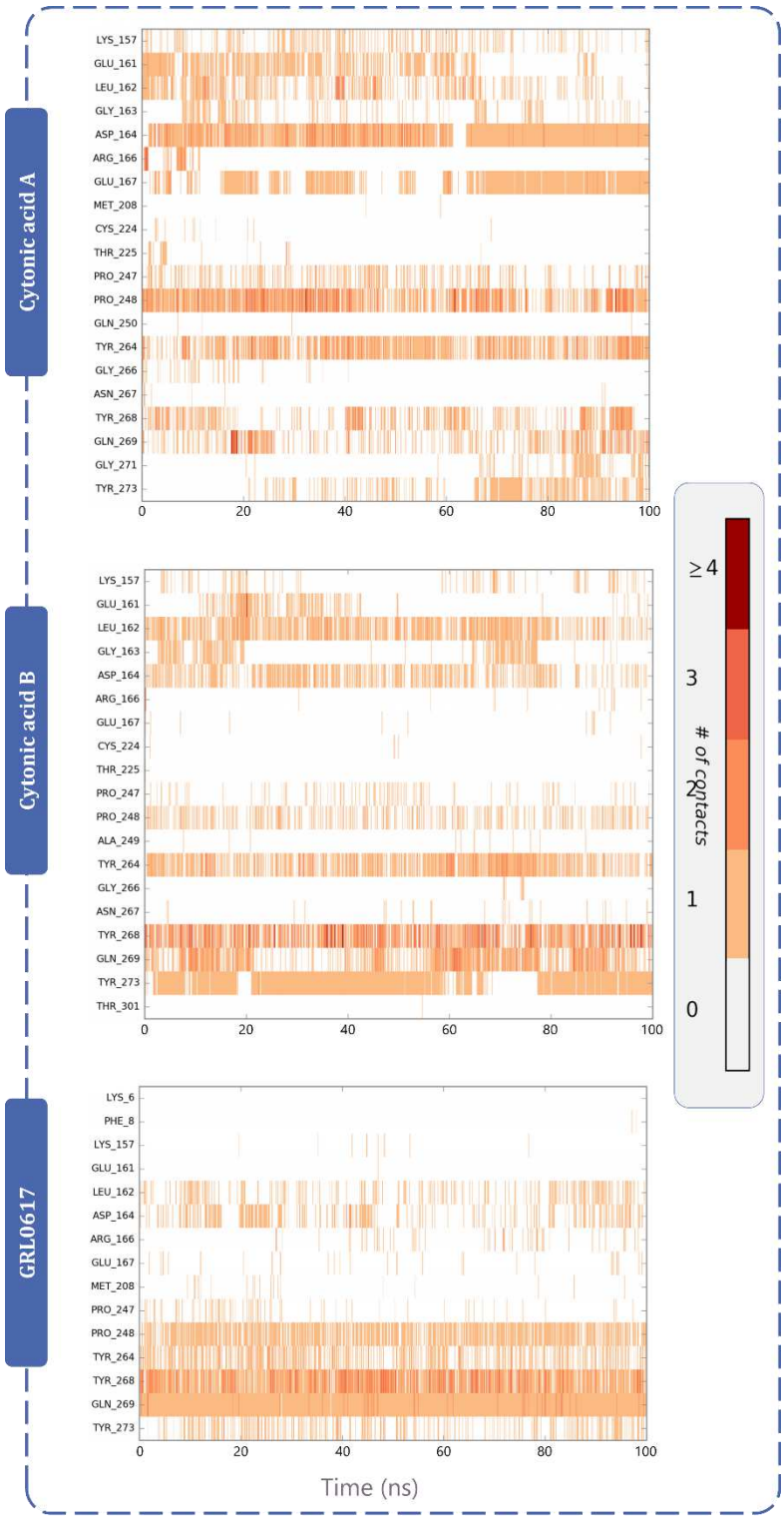

805

806 **Figure 11** Timeline representation of the interactions of ligand with amino acids for the
807 complex SARS-CoV2-PLpro-Cytonic acid A, SARS-CoV2-PLpro- Cytonic acid B and SARS-
808 CoV2-PLpro-GRL0617.

809

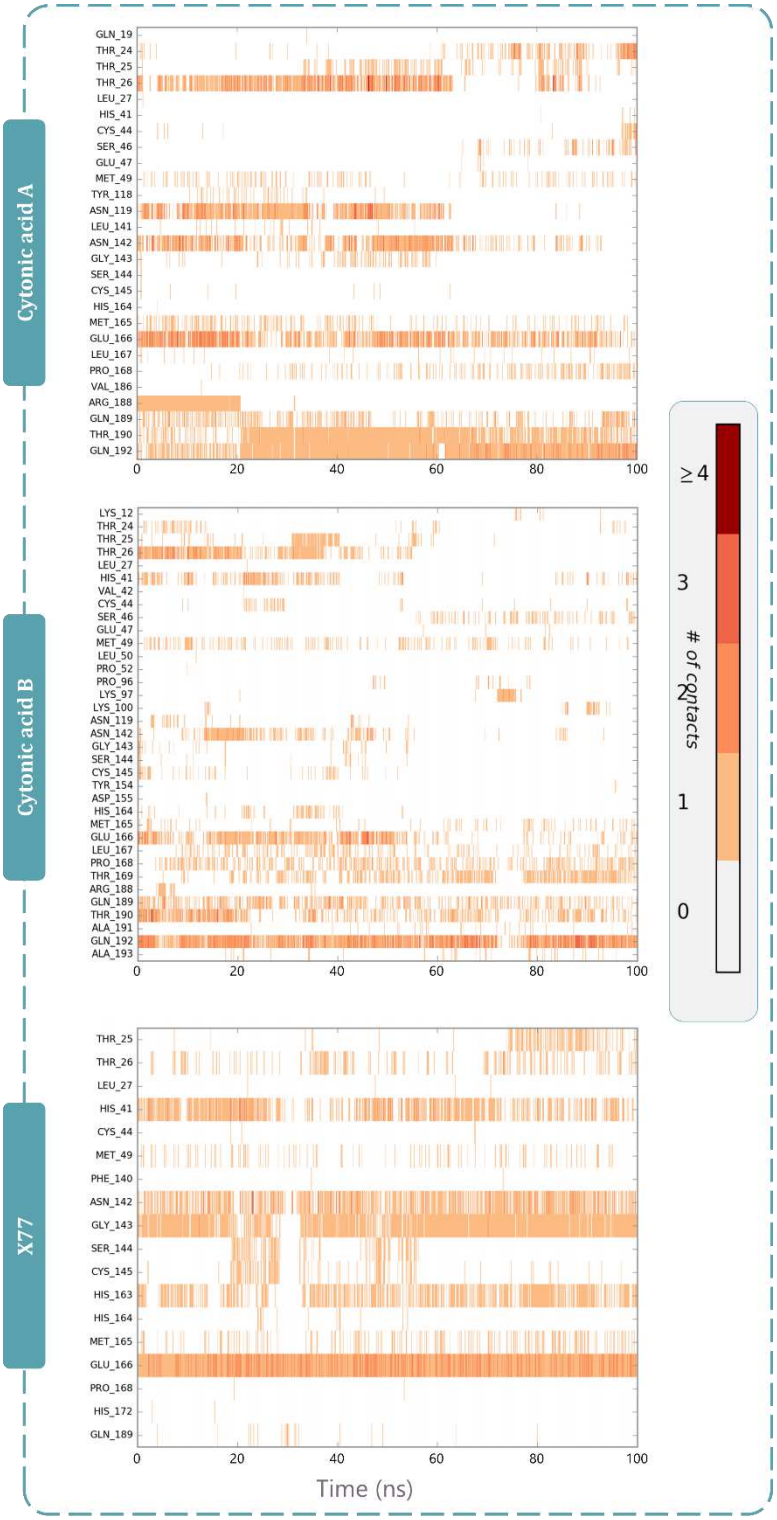

Figure 12 Timeline representation of the interactions of ligand with amino acids for the complex SARS-CoV2-Mpro-Cytonic acid A, SARS-CoV2-Mpro- Cytonic acid B and SARS-CoV2-Mpro-X77.

Tables

Table 1 List of antiviral compounds the endophytes with its Metadata

Sr. No.	Secondary metabolite	Endophytic organism	Host	Location	Virus	Activity (IC_{50})	Reference
1.	6-O-demethyl-4-dehydroxyaltersolanol A	*Nigrospora* sp. YE3033	*Aconitum carmichaeli*	China	H1N1 influenza A	2.59±1.22 µg/mL	22
2.	4-dehydroxyaltersolanol A					8.35±1.41 µg/mL	
3.	Altersolanol B					7.82±1.86 µg/mL	
4.	Chermesinone B					0.80±0.29 µg/mL	
5.	Emodin	*Aspergillus versicolor*	*Halimeda opuntia*	Egypt	HCV Protease	22.5 ± 1.6 µg/mL	15
6.	ω-hydroxyemodin	*Fusarium equiseti*	*Padina pavonica*	Egypt	HCV Protease	10.71 ± 2.3 µM	17
7.	(+)-Sclerotiorin	*Penicillium sclerotiorum* PSU-A13	*Garcinia atroviridis*	Thailand	HIV-1 Integrase	14.5 µg/mL	18
					HIV-1 Protease	62.7 µg/mL	
8.	Cordycepin	*Fusarium equiseti*	*Padina pavonica*	Egypt	HCV Protease	22.3 µM	17
9.	Ara-A					24.5 µM	
10.	Cyclic tetrapeptidecyclo-[Phenyl alanyl-pro-leu-pro]					29.4 µM	
11.	17-demethyl-2,11-dideoxy-rhizoxin					29.4 µM	
12.	5-chloro-3,6-dihydroxy-2-methyl-1,4-benzoquinone					34.4 µM	
13.	Perlolyrine					35.1 µM	
14.	Cyclo (L-Pro-L-Val)					23.2 µM	
15.	Griseoxanthone C					19.8 µM	

16.	Stachybogrisephenone B	*Stachybotry* sp. HH1 ZDDS1F1-2	Sponge	China	EV71	30.1 µM	[23]
17.	Grisephenone A					50.0 µM	
18.	3,6,8- Trihydroxy-1-methylxanthine					40.3 µM	
19.	Emerimidine A	*Emericella* sp. (HK-ZJ)	*Aegiceras corniculatum*	China	H1N1 influenza A	42.07 µg/mL	[24]
20.	Emerimidine B					62.05 µg/mL	
21.	Chloropupukeananin	*Pestalotiopsis fici*	Unknown	China	HIV-1	14.6 µM	[25]
22.	Periconiasin G	*Periconia* sp. F-31	*Annona muricata*	China	HIV-1	67.0 µM	[26]
23.	Aspergilline A	*Aspergillus versicolor*	*Paris polyphylla* var. *yunnanensis*	China	Tobacco mosaic virus	56.4 ± 3.8 µM	[27]
24.	Aspergilline B					47.3 ± 3.2 µM	
25.	Aspergilline C					35.6 ± 2.8 µM	
26.	Aspergilline D					38.9 ± 3.5 µM	
27.	Aspergilline E					33.6 ± 3.0 µM	
28.	Cytonic acid A	*Cytonaema* sp. F32027	*Quercus* sp.	U. K	CMV Protease	43 µM	[28]
29.	Cytonic acid B					11 µM	
30.	Phomopsone B	*Phomopsis* sp. CGMCC No.5416	*Achyranthes bidentata*	China	HIV-1	7.6 µM	[16]
31.	Phomopsone C					0.5 µM	
32.	Altertoxin V	*Alternaria tenuissima* QUE1Se	*Quercus emoryi*	USA	HIV-1	0.09 µM	[29]
33.	Altertoxin I					1.42 µM	
34.	Altertoxin II					0.21 µM	

35.	Altertoxin III					0.29 µM	
36.	Xiamycin	*Streptomyces* sp. GT2002/1503	*Bruguiera gymnorrhiza*	Germany	HIV-1	NA	[30]
37.	Xiamycin methyl ester					NA	
38.	Neosartoryadin A	*Neosartorya udagawae* HDN13-313	*Aricennia marina*	China	H1N1 influenza A	66 µM	[31]
39.	Neosartoryadin B					58 µM	
40.	Asperphenalenone A	*Aspergillus* sp. CPCC 400735	*Kadsura longipedunculata*	China	HIV-1	4.5 µM	[32]
41.	Asperphenalenone D					2.4 µM	
42.	Cytochalasin Z8					9.2 µM	
43.	Epicocconigrone A					6.6 µM	
44.	Alternariol 5-o-methyl ether	*Colletotrichum* sp.	NA	China	HIV-1	NA	[33]
45.	8-Methyl emodin	*Aspergillus versicolor*	*Halimeda opuntia*	Egypt	HCV Protease	40.2 ± 2.3 µg/mL	[15]

NA = Not Available

Table 2 Compounds managed to pass PLpro-GRL0167 complex pharmacophore hypothesis using Phase virtual screening

Entry	Compound name	Number of Sites Matched	Matched Ligand Sites	Phase Screen Score
1	Stachybogrisephenone B	4	A(3) D(7) D(8) R(14) R(-)	1.766
2	4-dehydroxyaltersolanol A	4	A(5) D(10) D(9) R(13) R(-)	1.723
3	Aspergilline D	4	A(3) D(10) D(11) R(-) R(17)	1.717
4	Altersolanol B	4	A(4) D(9) D(8) R(11) R(-)	1.669
5	Aspergilline E	4	A(3) D(12) D(13) R(-) R(20)	1.513
6	Cytonic acid B	4	A(4) D(12) D(-) R(21) R(20)	1.436
7	Perlolyrine	4	A(1) D(-) D(4) R(6) R(9)	1.435
8	Neosartoryadin A	4	A(3) D(-) D(8) R(12) R(11)	1.434
9	Asperphenalenone D	4	A(7) D(13) D(12) R(23) R(-)	1.419
10	Cordycepin	4	A(4) D(8) D(7) R(-) R(12)	1.400
11	Asperphenalenone A	4	A(6) D(9) D(8) R(22) R(-)	1.330
12	Cytonic acid A	4	A(3) D(9) D(-) R(19) R(20)	1.290
13	Altertoxin I	4	A(1) D(9) D(8) R(-) R(12)	1.244
14	Aspergilline A	4	A(6) D(9) D(7) R(-) R(15)	0.528
15	Aspergilline C	4	A(6) D(9) D(7) R(-) R(17)	0.505

Table 3 Compounds managed to pass Mpro-X77 complex pharmacophore hypothesis using Phase virtual screening

Entry	Compound name	Number of Sites Matched	Matched Ligand Sites	Phase Screen Score
1	Altertoxin V	4	A(1) A(2) R(12) R(-) R(13)	1.522
2	Epicocconigrone A	4	A(3) A(4) R(17) R(-) R(18)	1.428
3	Stachybogrisephenone B	4	A(4) A(6) R(-) R(14) R(15)	1.415
4	Altertoxin II	4	A(2) A(3) R(12) R(-) R(11)	1.39
5	Alternariol 5-O-methyl ether	4	A(3) A(4) R(11) R(-) R(12)	1.373
6	Emodin-8-methyl ether	4	A(4) A(1) R(10) R(-) R(11)	1.314
7	Emodin	4	A(4) A(3) R(11) R(-) R(10)	1.303
8	Altertoxin III	4	A(2) A(6) R(12) R(-) R(13)	1.285
9	Altertoxin I	4	A(2) A(4) R(13) R(-) R(12)	1.252
10	Griseoxanthone C	4	A(3) A(4) R(11) R(12) R(-)	1.235
11	Perlolyrine	4	A(1) A(2) R(7) R(6) R(-)	1.098
12	Asperphenalenone A	4	A(6) A(1) R(23) R(-) R(22)	1.094
13	Asperphenalenone D	4	A(9) A(5) R(24) R(-) R(23)	1.067
14	Altertoxin VI	4	A(1) A(3) R(11) R(-) R(12)	0.973
15	Cytonic acids A	4	A(5) A(9) R(-) R(21) R(22)	0.945
16	Neosartoryadin B	4	A(3) A(4) R(-) R(16) R(17)	0.939
17	Neosartoryadin A	4	A(2) A(5) R(16) R(15) R(-)	0.936
18	Cytonic acid B	4	A(6) A(8) R(22) R(21) R(-)	0.876

Table 4 Docking scores and the contributing binding residues of known PLpro inhibitor GRL-0617, Mpro inhibitor X77 and selected top antiviral metabolites generated using XP docking

Compounds	Glide Score (Kcal/mol)	Contributing Binding Residues
SARS-CoV2-PLpro		
GRL-0617 (Control)	-6.441	ASP164, GLN269, TYR268, TYR264, PRO247, PRO248, LEU162, GLY163, ARG166, MET208, TYR273, GLY271, CYS270, THR301
Aspergilline E	-7.77	PRO247, TYR268, ASP164, GLY163, GLY271, TYR264, LEU162, TYR273, GLN269, GLY266, PRO248, ASN267, THR301, MET208
Cytonic acid A	-7.655	GLU161, GLU167, LEU162, GLY163, ASP164, GLN269, CYS270, TYR264, TYR268, GLY266, PRO248, ASN267, MET208, ARG166, PRO247, GLY271, LYS157
Cytonic acid B	-7.292	PRO247, PRO248, TYR273, ASN267, TYR264, GLU167, GLY266, GLY163, GLU161, LEU162, GLN269, ASP164, TYR268, MET208
4-dehydroxyaltersolanol A	-6.859	PRO247, PRO248, TYR273, ASP164, GLY163, GLN269, GLU167, LYS157, LEU162, TYR268, TYR264, THR301
SARS-CoV2-Mpro		
X77 (Control)	-8.52141	MET49, ASP187, ARG188, PRO52, VAL42, CYS44, HIS41, THR25, LEU27, THR26, CYS145. ASN142, GLY143, SER144, HIS163, PHE140, LEU141, GLU166, HIS172, LEU167, TYR54, HIS164, GLN189, MET165, PRO168
Cytonic acid B	-9.998	HIS41, ASP187, GLY170, GLU166, LEU167, ALA191, GLN192, GLN189, THR190, PRO168, ARG188, MET165, CYS145, ASN142, MET49, THR25, THR24, SER46, LEU27, GLY143, HIS164, THR26, TYR54
Cytonic acid A	-9.798	CYS44, PRO52, MET49, TYR54, HIS41, ASN142, THR26, THR24, THR25, ASN119, GLY143, TYR118, LEU27, SER46, THR45, VAL42, GLU166, LEU167, PRO168, THR190, GLN192, ARG188, GLN189, HIS164, MET165, ASP187, ASP48
Asperphenalenone D	-8.969	MET165, VAL186, HIS164, MET49, CYS44, THR45, SER46, THR25, THR24, GLY143, THR26, LEU27, CYS145, ASN142, SER144, GLN189, ASP187, PRO168, ALA191, THR190, LEU167, GLN192, ARG188
Asperphenalenone A	-6.2417	MET165, CYS44, ARG188, GLN189, MET49, ASN28, LEU27, VAL42, THR26, ASN119, GLY143, LEU141, TYR118, ASN142, THR25, THR24, SER46, HIS41, HIS163, SER144, CYS145, GLU166

Table 5 Structural and Chemical properties of screened antiviral compounds.

Name of the Compounds	Structure	Molecular Weight	LogP	#Rotatable Bonds	#Acceptors	#Donors	Surface Area
GRL0617	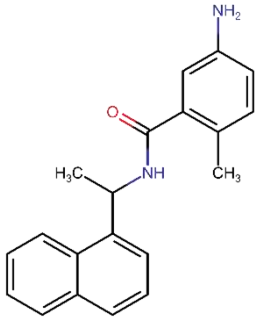	304.393	4.22142	3	2	2	135.68
X77	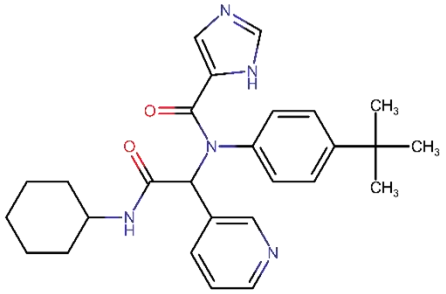	459.594	4.9392	6	4	2	200.565
Cytonic acid A	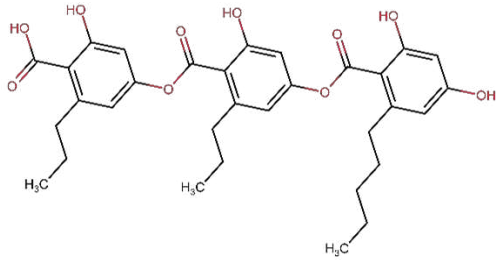	580.63	6.2833	13	9	5	243.338

Cytonic acid B	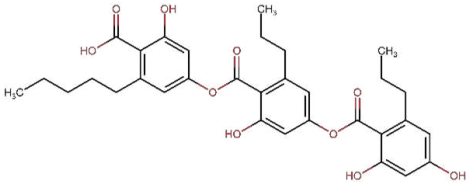	580.63	6.2833	13	9	5	243.338
Aspergilline E	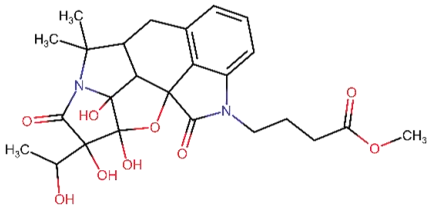	502.52	-0.8761	5	9	4	206.744
4-dehydroxyaltersolanol A	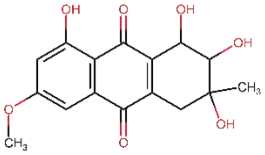	320.297	-0.0471	1	7	4	130.993
Asperphenalenone D	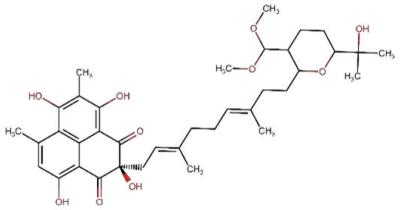	654.797	6.08024	12	10	5	276.210
Asperphenalenone A	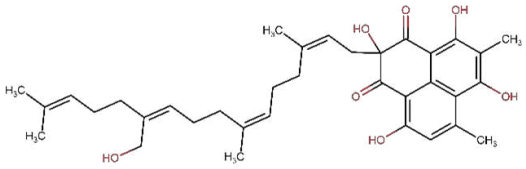	576.73	7.19174	12	7	5	247.767

Table 6 MM-GBSA binding free energy change profiles of ligands with SARS-CoV2-PLpro and SARS-CoV2-Mpro for docked complexes.

Ligand	ΔGBind (Kcal/mol)	ΔGCoulomb (Kcal/mol)	ΔGHbond (Kcal/mol)	ΔGLipo (Kcal/mol)	ΔGPacking (Kcal/mol)	ΔGvdW (Kcal/mol)
Ligands interacting with SARS-CoV2-PLpro						
GRL-0617 (Control)	-67.5637	-20.1695	-2.5442	-26.1400	-3.1440	-46.3768
Aspergilline E	-50.8186	-17.1949	-1.24148	-18.2587	-0.54685	-35.848
Cytonic acid A	-58.9626	-34.7886	-2.45573	-20.7273	-2.897	-42.5047
Cytonic acid B	-55.6721	-28.8001	-1.74414	-25.71	-3.10166	-52.1166
4-dehydroxyaltersolanol A	-38.3654	-22.0615	-3.34432	-14.1614	-1.84419	-31.2361
Ligands interacting with SARS-CoV2-Mpro						
X77 (Control)	-79.8911	-35.3714	-1.8857	-17.6157	-3.0805	-59.5617
Cytonic acid A	-75.3087	-36.7368	-4.0966	-16.7277	-0.5834	-58.2717
Cytonic acid B	-67.6847	-41.9421	-3.7410	-13.1996	-1.6820	-54.3987
Asperphenalenone D	-65.9103	-24.9700	-2.4700	-16.5780	-1.7280	-50.2750
Asperphenalenone A	-50.4602	-10.6094	-1.8999	-11.8471	-2.2800	-52.6731

Note, meaning of abbreviations used in the table are as follows:
Coulomb—Coulomb energy
Hbond—Hydrogen-bonding correction
Lipo—Lipophilic energy
Packing—Pi-pi packing correction
vdW—Van der Waals energy

Table 7 ADMET properties of screened antiviral compounds.

Property	Model Name	Predicted values								Unit
		GRL0617	X77	Cytonic acid A	Cytonic acid B	Aspergilline E	4 dehydroxyal tersolanol A	Asperphen alenone D	Asperphen alenone A	
Absorption	Water solubility	-4.678	-2.878	-2.902	-2.914	-2.639	-2.009	-3.495	-3.746	Numeric (log mol/L)
Absorption	CaCO2 permeability	1.302	1.29	-1.108	-1.17	0.697	0.633	-0.093	-0.172	Numeric (log Papp in 10^{-6} cm/s)
Absorption	Intestinal absorption (human)	92.815	89.686	46.99	62.692	56.317	67.204	76.573	79.961	Numeric (% Absorbed)
Absorption	Skin Permeability	-2.785	-2.735	-2.735	-2.735	-2.735	-2.848	-2.735	-2.735	Numeric (log Kp)
Absorption	P-glycoprotein substrate	Yes	Yes	Yes	Yes	Yes	Yes	Yes	Yes	Categorical (Yes/No)
Absorption	P-glycoprotein I inhibitor	No	Yes	No	No	Yes	No	Yes	Yes	Categorical (Yes/No)
Absorption	P-glycoprotein II inhibitor	Yes	Yes	No	No	No	No	Yes	Yes	Categorical (Yes/No)
Distribution	VDss (human)	0.086	0.656	-1.267	-1.707	0.431	-0.006	0.454	-0.357	Numeric (log L/kg)
Distribution	Fraction unbound (human)	0	0.262	0.08	0.006	0.373	0.413	0.056	0.013	Numeric (Fu)
Distribution	BBB permeability	0.055	-0.899	-1.896	-1.782	-0.969	-0.844	-1.67	-1.404	Numeric (log BB)
Distribution	CNS permeability	-1.604	-2.31	-3.143	-3.183	-3.826	-3.494	-3.054	-2.722	Numeric (log PS)
Metabolism	CYP2D6 substrate	No	No	No	No	No	No	No	No	Categorical (Yes/No)
Metabolism	CYP3A4 substrate	Yes	No	No	No	No	No	Yes	Yes	Categorical (Yes/No)
Metabolism	CYP1A2 inhibitor	Yes	No	No	No	No	No	No	No	Categorical (Yes/No)

Metabolism	CYP2C19 inhibitor	Yes	No	No	No	No	No	No	No	Categorical (Yes/No)
Metabolism	CYP2C9 inhibitor	Yes	No	No	No	No	No	No	No	Categorical (Yes/No)
Metabolism	CYP2D6 inhibitor	No	No	No	No	No	No	No	No	Categorical (Yes/No)
Metabolism	CYP3A4 inhibitor	Yes	Yes	No	No	No	No	Yes	Yes	Categorical (Yes/No)
Excretion	Total Clearance	0.221	0.671	0.268	0.183	0.143	0.453	-0.035	0.071	Numeric (log ml/min/kg)
Excretion	Renal OCT2 substrate	No	Yes	No	No	No	No	No	No	Categorical (Yes/No)
Toxicity	AMES toxicity	Yes	Yes	No	No	No	No	No	No	Categorical (Yes/No)
Toxicity	Max. tolerated dose (human)	-0.043	0.601	0.44	0.467	-0.645	-0.078	0.229	0.191	Numeric (log mg/kg/day)
Toxicity	hERG I inhibitor	No	No	No	No	No	No	No	No	Categorical (Yes/No)
Toxicity	hERG II inhibitor	Yes	Yes	No	No	No	No	Yes	Yes	Categorical (Yes/No)
Toxicity	Oral Rat Acute Toxicity (LD50)	2.472	2.396	2.499	2.444	2.302	1.923	2.253	2.042	Numeric (mol/kg)
Toxicity	Oral Rat Chronic Toxicity (LOAEL)	0.462	1.528	2.897	2.891	3.695	2.734	1.602	2.462	Numeric (log mg/kg_bw/ day)
Toxicity	Hepatotoxicity	No	Yes	No	No	No	No	No	No	Categorical (Yes/No)
Toxicity	Skin Sensitisation	No	No	No	No	No	No	No	No	Categorical (Yes/No)
Toxicity	*T. pyriformis* toxicity	0.529	0.285	0.285	0.285	0.285	0.287	0.285	0.286	Numeric (log ug/L)
Toxicity	Minnow toxicity	1.936	2.563	1.089	0.011	4.392	4.044	-2.806	-4.272	Numeric (log mM)